International Forum on Aeroelasticity and Structural Dynamics
IFASD 2019
9-13 June 2019, Savannah, Georgia, USA

IMPROVING PIEZOELECTRIC ENERGY HARVESTING FROM AN AEROELASTIC SYSTEM

Dani Levin[1], Earl H. Dowell[2]

[1]Department of Mechanical Engineering and Material Science
Duke University
Durham, NC 27708-0300 USA
dowell@ee.duke.edu

[1]Department of Mechanical Engineering and Material Science
Duke University
Durham, NC 27708-0300 USA
dani.levin@duke.edu

Keywords: piezoelectricity, flutter, LCO, energy-harvesting, non-linearity, flag

Abstract: Our experimental study sought to answer the question: how to maximize the piezoelectric power extraction of an aeroelastic system?
A simple rectangular cantilever plate, which experiences non-linear aeroelastic limit cycle oscillations (LCO), was used as a basic vibrating system. The plate was covered entirely with piezoelectric elements on both sides.
By adding small discrete masses along the plate, we were able to increase the power generation efficiency by 260% while reducing the airspeed required to produce this power, from 23.5 m/sec to 15.1 m/sec, and the level of vibrations from 77 g to 24 g. Moreover, the energy harvester can be exploited over a wide range of air speeds without structural failure.
Our experiments show several surprising results:

- With proper mass placement, piezo-elements near the tip of the vibrating plate can generate more power that those near the root.
- The increased damping of the system contributes to a more efficient and sustainable power generator.
- For a power generator which is based on an elastic structure which experience large deflections, the use of PVDF piezo-elements is advantageous, as opposed to more efficient ceramic based elements.

Our goal for this work is to contribute to a more practical piezoelectric energy harvesting solution based on aeroelastic effects.

1 INTRODUCTION

Remotely located electronic devices, such as wireless sensors, transmitters and monitoring units, are constantly being developed and deployed. These devices have become more efficient and as a result require less power to operate. This opens possibilities for ambient energy harvesters (EH) to be paired with such devices to make them self-sufficient over long time periods [1], and might be more suitable for these purposes than batteries which are currently used [2]. In the micro watt range, piezoelectric elements, which convert vibrations into electric energy, have become common [1], [3]. The simplest example of an EH device is a vibrating cantilever beam with piezoelectric elements attached at the root [4], [5], [6]. To achieve favorable energy generation, the physical properties of the beam, i.e. the material, length, cross section dimensions and the tip proof mass, can be tuned according to the available ambient energy sources

Flow induced vibrations arising from fluid-structure interaction, or aeroelastic effects, are considered as one of the most promising potential sources of energy [2]. These vibrations can be obtained from natural-flow conditions, are self-excited and thus more feasible and scalable than forced vibrations. Combining piezoelectric elements with aeroelastic effects can lead to attractive and efficient EH devices, see [2], [7], [8] for comprehensive reviews. Aeroelastic effects, such as flutter, are usually undesirable phenomena in any aircraft/structure design. However, while linear flutter is a one-time destructive occurrence, non-linear incidents, such as Limit Cycle Oscillations (LCO) may not cause structural damage. LCO can sustain finite amplitude vibrations for long time periods and thus can be exploited for energy harvesting purposes.

Power generation from LCO can take several forms. The most common would be attaching piezo-element to the root of a flexible vibrating plate, see [9] for an example. In another variation, a rigid airfoil is used. The airfoil is mounted on non-linear springs which are tuned to result in LCO. The piezo-elements in this case are attached to the leaf springs which vibrate while the rigid airfoil oscillates [10], [11]. An interesting combined approach uses a flexible beam with a pin connected rigid flap [12]. The divergent coupling between the flap in pitch with large rotations angles, and large deflections of the beam in bending drive piezoelectric elements, which are attached to the root of the beam. In [13] a 2D airfoil with 2 Degrees of Freedom (DOF) is investigated. Free play nonlinearity is introduced in the pitch DOF, and the piezo elements are attached to the linear leaf springs in the plunge DOF. The model was explored both theoretically and experimentally to optimize for resistive load and the power output. The study shows that the load resistance mainly influences the power output and not the mechanical motion of the system.

Previously mentioned work used discrete piezo-elements which are driven by the larger oscillating structure. When the goal is to increase the power output, the location of piezo-elements and the number of such elements must be considered. In recent research [14], newly developed computational models show promising levels of harvested electric power when the entire plate is covered with piezoelectric elements. A theoretical and experimental study which explored the optimal placement of piezoelectric elements along flapping flag is described in [15]. Installing the elements in areas of large curvature led to increased power output. This is especially significant on a small scale where the stiffnesses of the substrate and the piezo elements are comparable. This was further explored in [16] where segmentation of the piezo elements was studied. The authors found that for increased power output, the nodal points of the vibrating mode should be outside of the elements – at the segmentation. This will alleviate the effect of cancellation when the element deflects. The authors also noted that finding such points for general oscillatory motion is not an easy task. Yet, an effort should be made to segment the elements closer to the estimated position of these nodes.

Our work is based on an aluminum plate which experiences LCO in the wind tunnel. The plate is larger compared to [15] or [16], and thus has lower frequency dynamics. In order to exploit the full potential of the structure, the plate is fully covered with piezoelectric elements on both sides. The generated voltages from chordwise located elements are rectified and then combined in parallel to maximize the power output [17]. This is better suited for power extraction from a large number of piezo elements [18], as opposed to locally adjusted segmentation like in [16]. The rectification is realized with a simple full-wave diode bridge [19], [20].
We studied changing the dynamics of the plate by adding small discrete masses in several locations, as in [21]. Our experience was consistent with the results for "long" plates, i.e. adding masses destabilizes the system, resulting in lower margins of flutter and LCO [21].
Unlike conventional aeroelastic systems, destabilizing can be beneficial for energy harvesting; the power is generated at lower air speeds, the system becomes more efficient and the generator is more sustainable. In this work we explored these effects to improve energy generation from an existing structure. We hope this work will contribute to a realization of a piezoelectric energy harvester based on aeroelastic effects.

2 EXPERIMENTAL SETUP

The flexible vibrating plate is made from 6061-T6 Aluminum. The area exposed to the flow has dimensions of 513mm long and 101.6mm wide; the thickness is 0.375mm. The plate is cantilevered from a stiff aluminum base profile, which is attached to the floor of the wind tunnel. See *Figure 1*. The vertical profile is covered with an aerodynamic 3d printed shroud to reduce vortex shedding over the plate.

2.1 Instrumentation

A small accelerometer, PCB 352C22, is located at the tip of the plate and midspan. The airspeed is measured using a pitot-tube with differential pressure sensor. The plate is covered with 24 piezo elements – DT4-028K/L (12 on each side), manufactured by TE connectivity (www.te.com). The area of the element measures 171x22mm with an active area of 156x19mm. Piezo elements were bonded to the aluminum plate using epoxy resin. The elements are divided into 6 separate "blocks", with 4 elements in each block. See *Figure 2*. Elements in each block are electrically connected in parallel, with a single output [17]. The data is acquired using a m+p VibPilot DAQ unit. The instrument is limited to a 10V maximum input, and the signal is clipped beyond this value. To overcome this limitation, we used a simple voltage divider with identical value resistors. The resultant voltage over a single resistor is recorded. Later the total voltage output is calculated by multiplying the recorded value by the number of resistors in the voltage divider. The total resistance is also summed up. m+p Analyzer software was used for data acquisition and analysis.

2.2 AC to DC Rectification

During vibration, piezoelectric elements generate AC voltage and current. DF04S full wave rectifier with smoothing capacitor was used to obtain DC voltage and measure it over a load resistor. See *Figure 3*. The DC output was measured with the same VibPilot DAQ instrument. The output voltage was recorded in two ways: once separately for each block and once with the 6 blocks combined in parallel, after rectification, and then recorded [18]. The two methods gave comparable results.

2.3 Load Resistor Values

In this work, values of 600-900 kΩ were used for the load resistors. Preliminary tests show increased power extraction for these values.

2.4 Power Calculation Formula

Once the voltage over load resistor is recorded, the power output can be calculated as follows:

$$P = {V^2}/{R} \tag{1}$$

Where: P – power
V – voltage
R – resistance

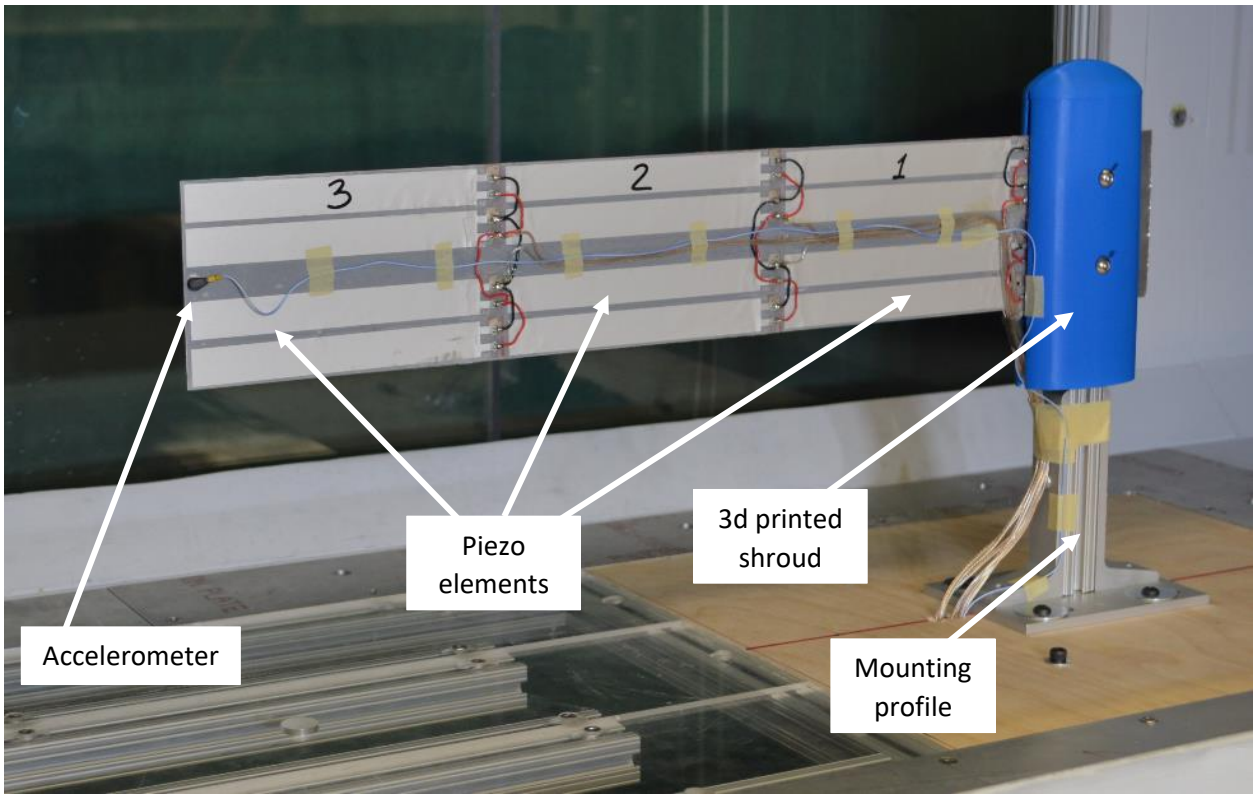

Figure 1: Wind Tunnel Test Setup (Fully covered plate shown)

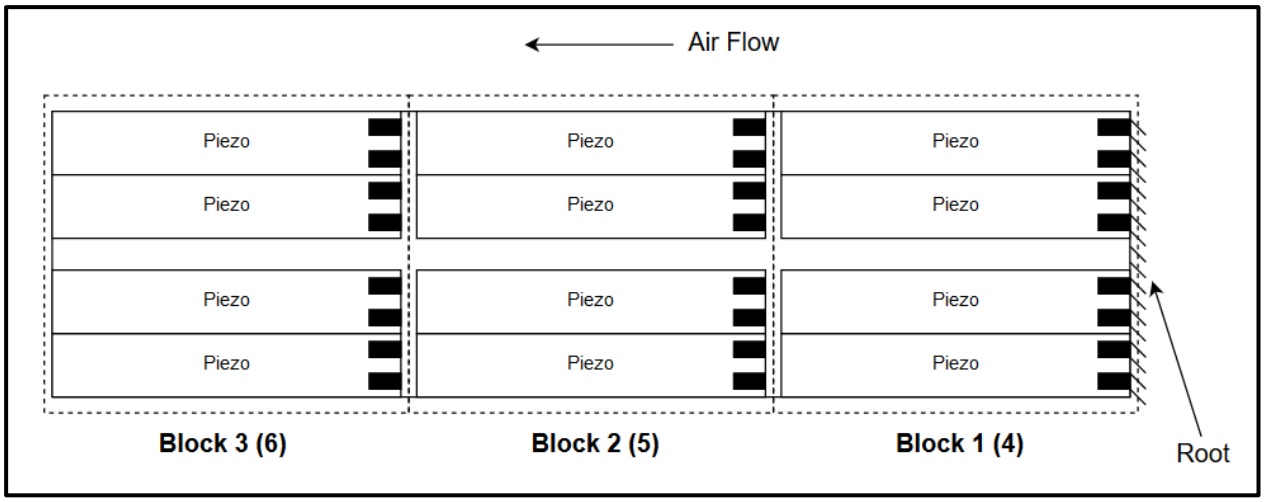

Figure 2: Block Numbering – Front (Back)

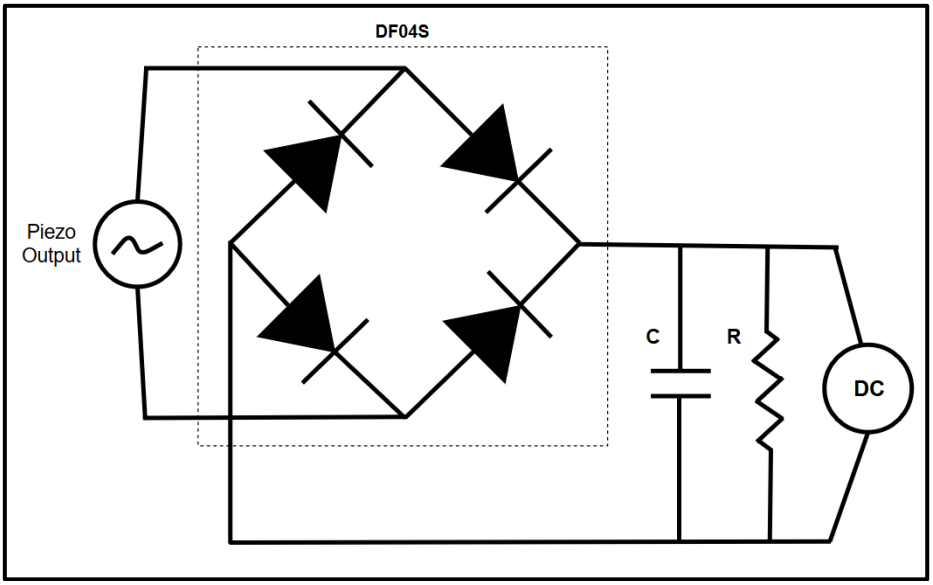

Figure 3: AC to DC Rectification, DC Output is Recorded

3 PRELIMINARY ANALYSIS

3.1 Modal Analysis

Finite Element (FE) modal analysis was performed to determine the natural frequencies and modes of the structure. ANSYS finite element commercial software was used for the calculations.

3.2 Flutter Analysis

The results from modal analysis were used as a structural model to perform a preliminary flutter analysis of the plate. A linear, potential flow, commercially available aerodynamic and aeroelastic code, ZAERO, was used.

4 TEST PROCEDURE

4.1 Flutter Test

The plate is placed in the wind tunnel in a flag orientation. See *Figure 1*. The air speed in the tunnel was increased until the plate starts oscillating. Usually oscillations occurred

spontaneously. However, in several instances the plate was deflected from its initial position, by an external rod, to induce the vibrations. The air speed was increased further until the tip acceleration reached ~100g, or the vibrations became too violent. Then the speed was decreased to 0. The data was recorded throughout the whole experiment at a 256Hz sampling rate.

4.2 Modal Test

A basic Experimental Modal Analysis (EMA) of the plate was performed. A PCB 086C01 modal hammer was used to tap the root and the response was recorded with the tip accelerometer, PCB 352C22. The recordings were used to determine the natural frequencies and modes of the actual configuration.

5 ESTABLISHING A BASE LINE

The first step is understanding our mechanical and electrical system: the modal dynamics and aeroelasticity, both for the empty and the fully covered plates, and potential power output for the fully covered plate. See *Figure 4*. Later configurations will be compared to the data established in this step.

5.1 Modal and Flutter Analyses

First four natural frequencies and mode shapes are shown in *Figure 5*. Flutter analysis shows a flutter mechanism which involves the first and second bending modes. The system becomes unstable at 14.1 m/sec with second bending being the dominant mode shape. See *Figure 6*. The flutter frequency is 5.4 Hz. We assumed 1% of structural damping in the flutter computations.

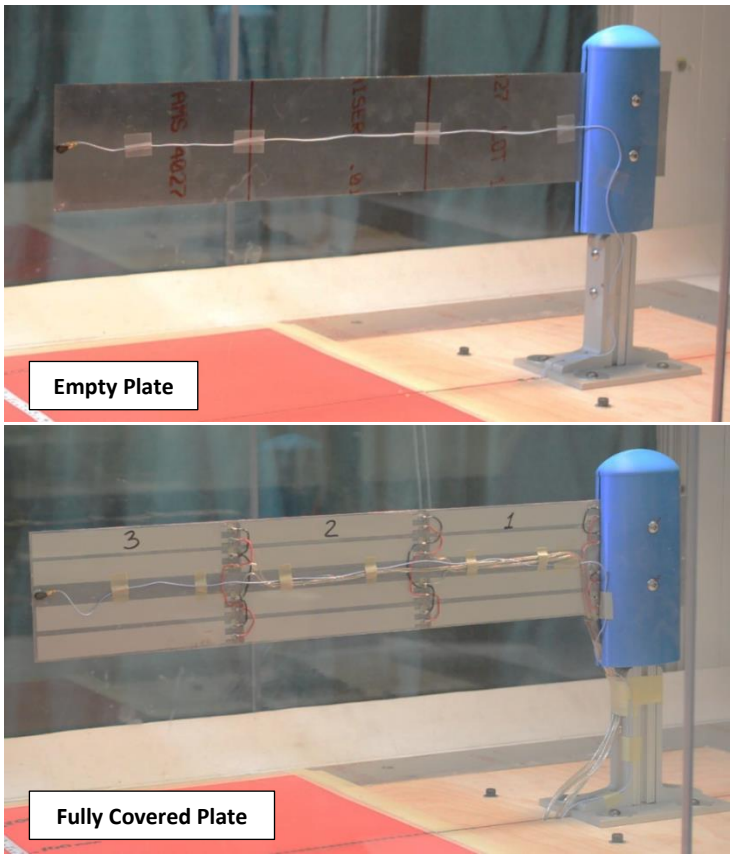

Figure 4: Base Line Configuration – Empty and Fully covered Plates

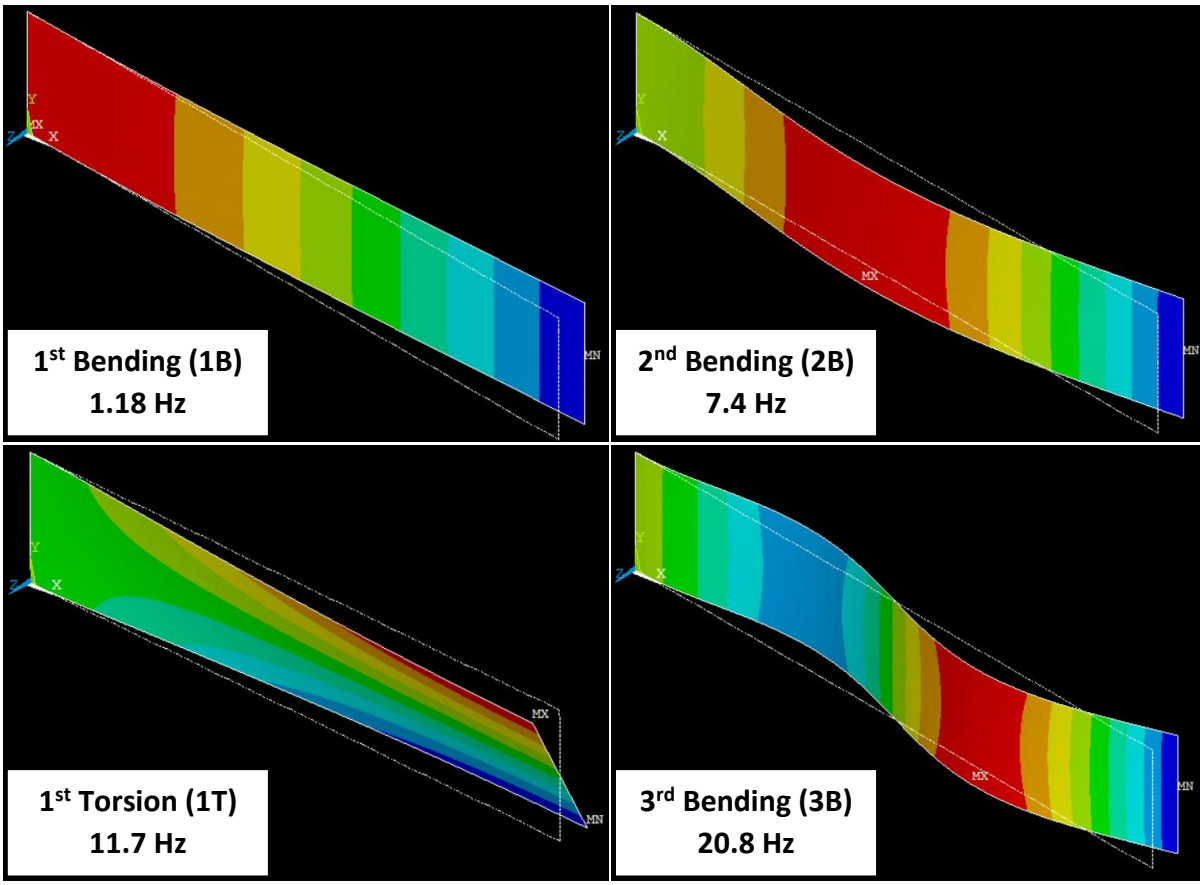

Figure 5: Modal Analysis Results – Empty Plate

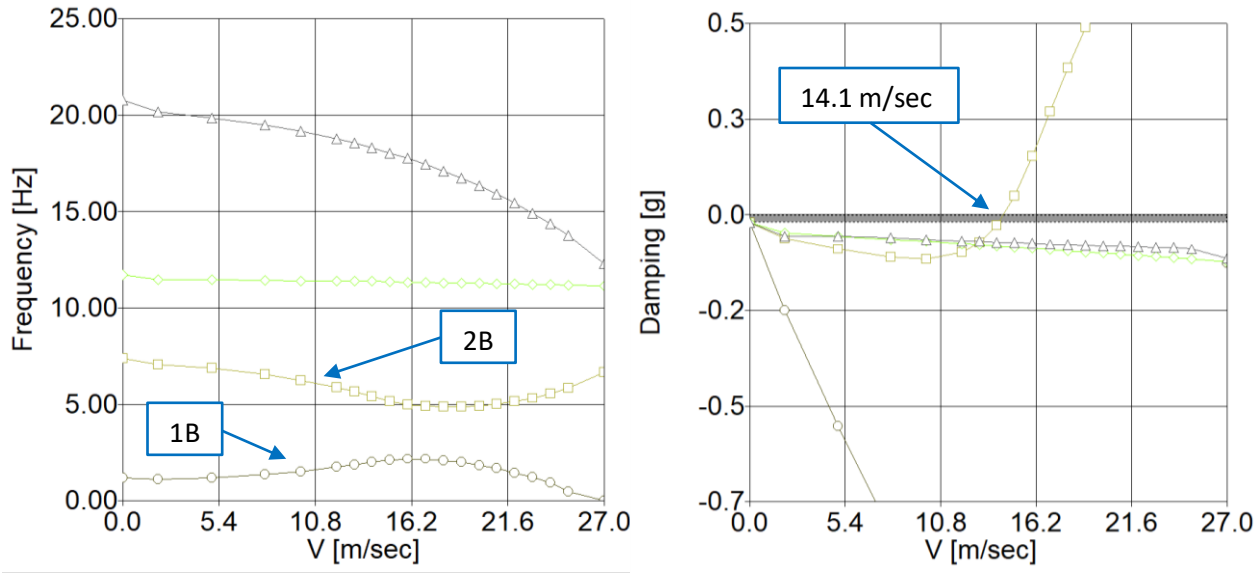

Figure 6: VG Plot (Frequency and Damping vs. Air Speed) for the Empty Plate

5.2 Experimental Results

Experimental modal frequencies and damping ratios of the two plates are compared to the theoretical results in *Table 1*. The values compare well for the empty plate. Note the increased stiffness (and hence frequency) and damping for the fully covered plate, as well as increased mass. Same trend is evident in the Frequency Response Function (FRF) plot. See *Figure 7*. This

change comes from the added piezo elements, wiring, and the epoxy layer which bonds the elements to the plate. A fully covered plate adds 68.7 gr to the empty plate mass of 66.7 gr.

Table 1: Dynamic Properties of the Plates

Mode	FE	Experimental Modal Analysis			
		Empty Plate		Fully Covered Plate	
	f [Hz]	f [Hz]	Damp [%]	f [Hz]	Damp [%]
1B	1.18	1.16	2.2	1.44	1.74
2B	7.4	7.46	0.74	9.95	1.6-3.3
1T	11.7	12.16	0.76	11.92	1.32
3B	20.8	21.08	0.44	22.87	6-6.8

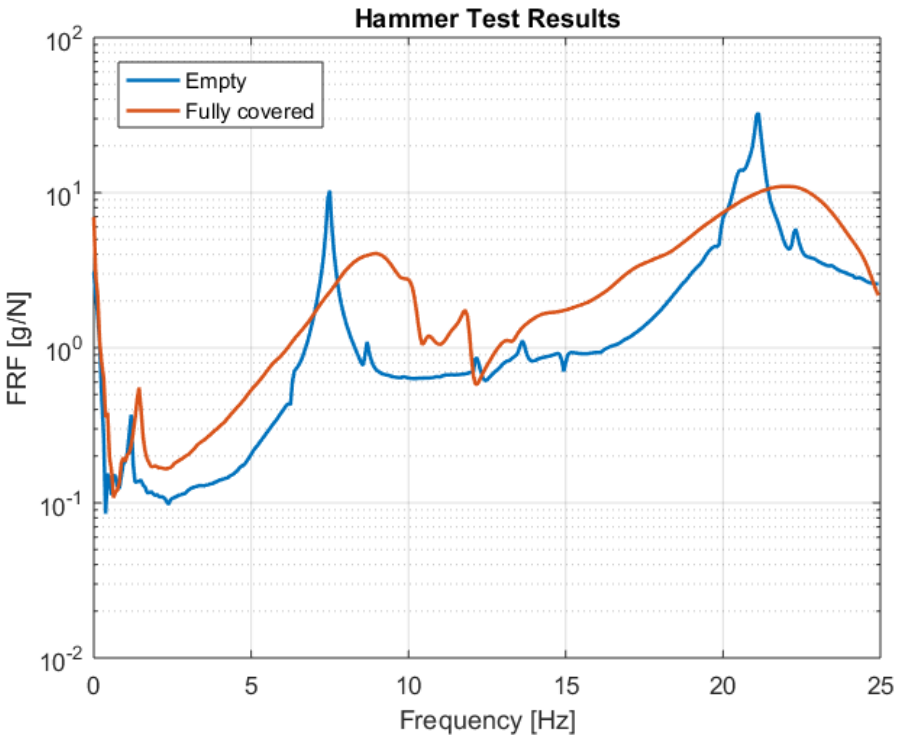

Figure 7: Experimental FRFs for Two Configurations

The tip acceleration vs. air speed, for the empty plate, is shown in *Figure 8*. Limit Cycle Oscillations (LCO) start at 18.1 m/sec, where the acceleration jumps quickly from 4.6g to 53g. This is larger than the predicted 14.1 m/sec, see *Figure 6*. The difference, here and throughout the paper, can be attributed, in part, to the fact that ZAERO is a linear code, while our experiments show highly non-linear behavior of the plate. In [22] a non-linear structural model of this plate was coupled with linear aerodynamic model. This analysis showed closer correlation with the experimental data. We stopped increasing the air speed at ~20 m/sec when the acceleration reached 105g. A small hysteresis was observed while reducing the speed; the LCO stopped at 15.9 m/sec, 2.2 m/sec below the initiation at 18.1 m/sec. This hysteretic behavior was observed throughout the tests, with increased hysteretic velocity increment for the fully covered plate.

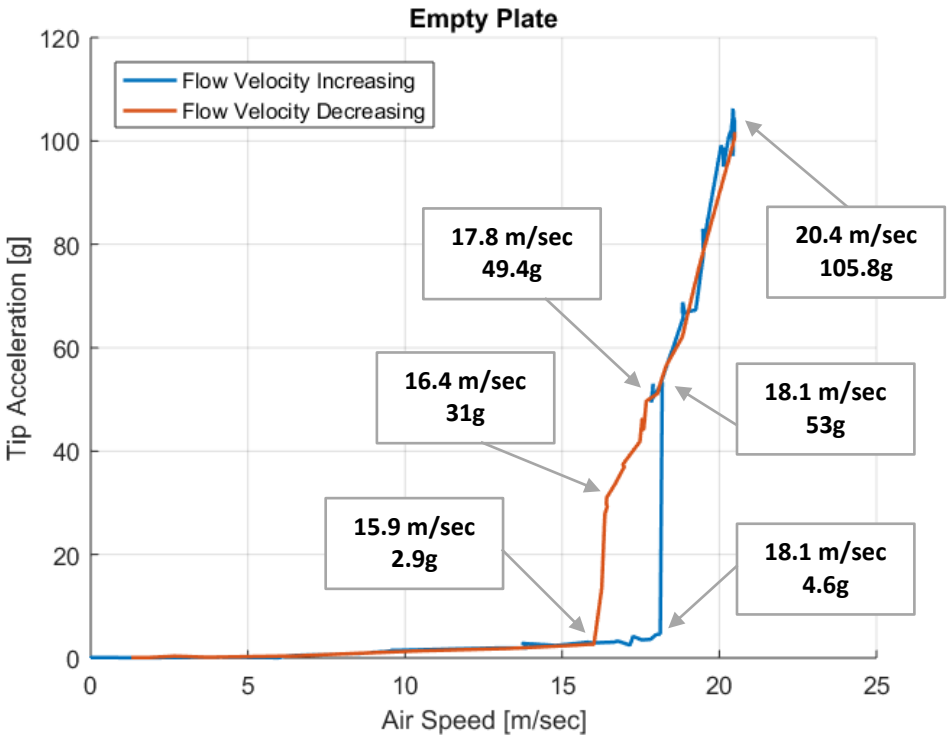

Figure 8: Flutter Test of an Empty Plate

For a fully covered plate, a different behavior was observed. Two ways of initiating LCO were used: increasing the air speed until the plate vibrates (as in the case with the empty plate) and deflecting the plate from its initial position at lower speeds to start the vibrations. In the first case the LCO initiation occurred at 35.9 m/sec with a large observed hysteresis increment in flow velocity – 16.1 m/sec, i.e. the vibrations stopped at 19.8 m/sec. See *Figure 9*. When deflecting the plate, a lower flow velocity for LCO initiation is possible – the plate starts to vibrate at 23.5 m/sec, with a smaller hysteresis increment in flow velocity of 5.2 m/sec for stopping the vibrations. See *Figure 10*. In both cases the "LCO stop" air speed is comparable, i.e. 19.8 vs. 18.3 m/sec.

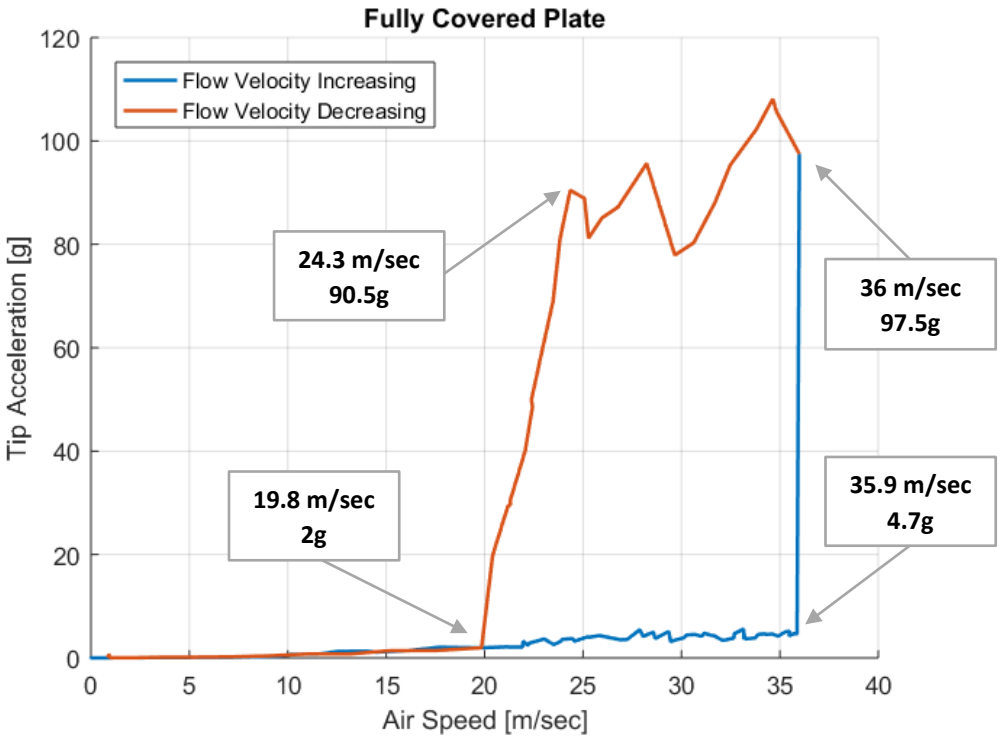

Figure 9: Flutter Test of a Fully Covered Plate, Natural Excitation

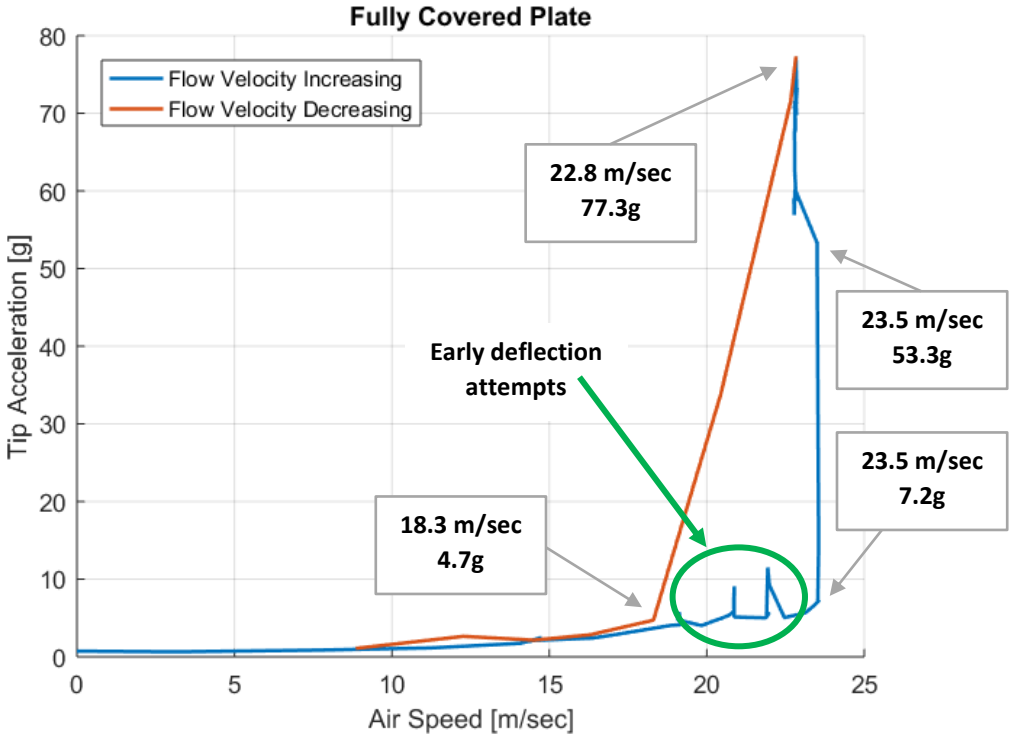

Figure 10: Flutter Test of a Fully Covered Plate, Deliberately Disturbed Excitation

The maximum power output for this plate is ~700-1000 μW. *Figure 11* shows a combined output from the whole plate, and the block by block output is shown in *Figure 12*. The significant output occurs when the plate is in LCO, as can be seen from the tip acceleration curve. The maximum power output occurs at blocks 2, 5 where the piezo elements experience

the largest bending curvature while in LCO. The output from tip blocks 3, 6 is the lowest, due to the minimal bending of 1B and 2B modes at the tip.

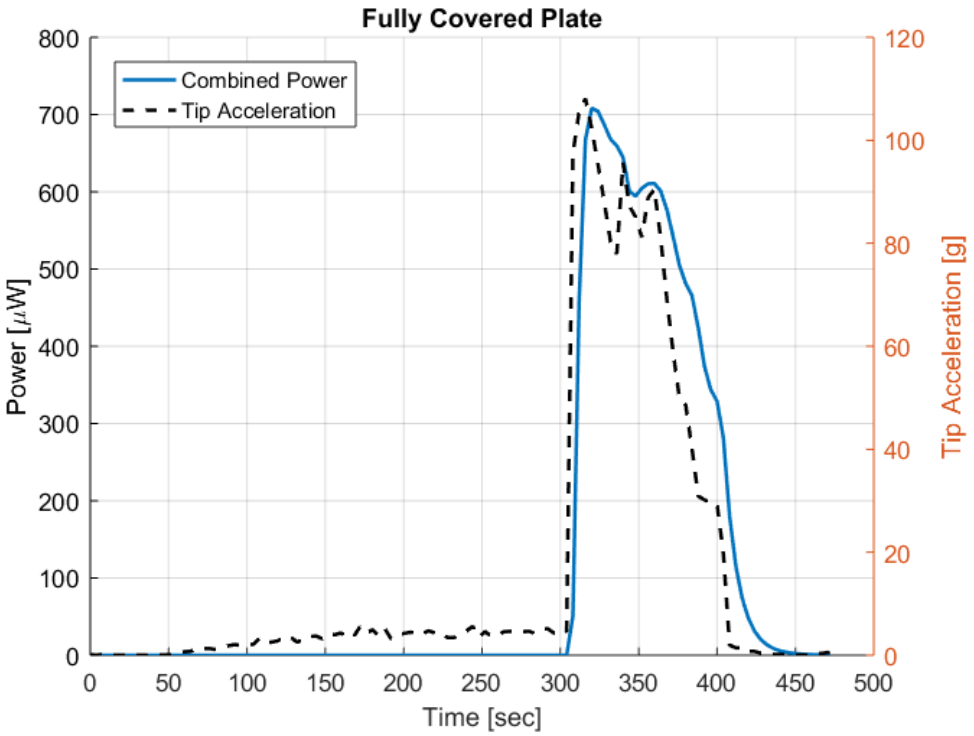

Figure 11: Combined Output from Fully Covered Plate

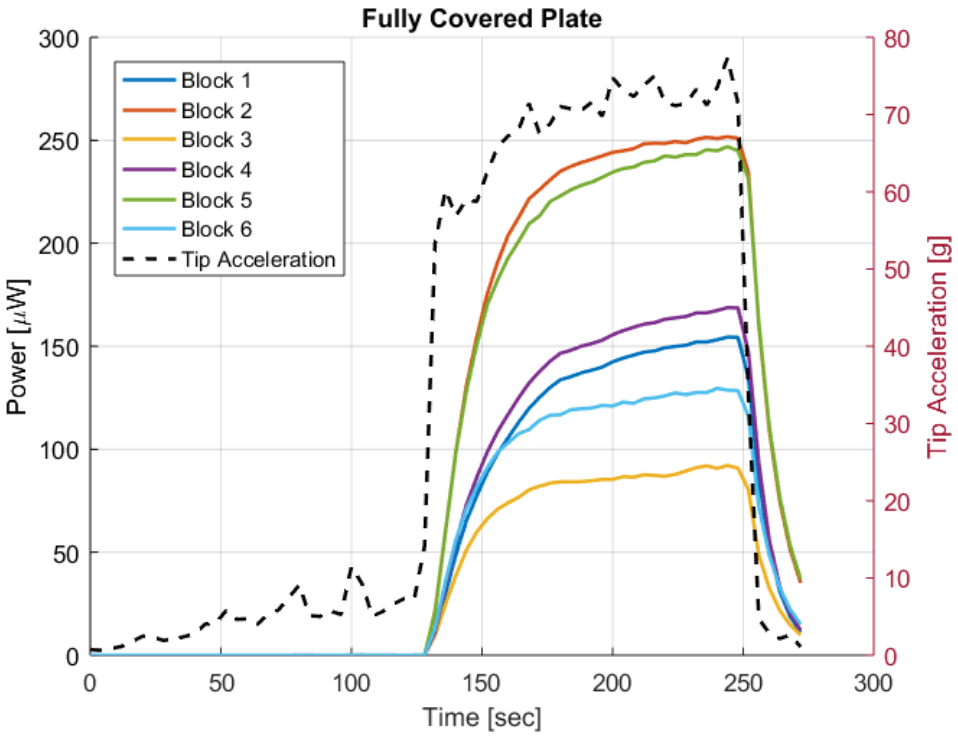

Figure 12: Block by Block Output from Fully covered Plate

6 IMPROVING POWER OUTPUT

To increase the power output from our system and to make it more practical, several changes can be made:

- Increase the vibration frequency.
- Increase the vibration amplitude.
- Create more curvature in the vibrational motion.
- Use more efficient piezo elements.
- Reduce the required air speed for LCO

We want to maintain the basic aeroelastic system, therefore the LCO mechanism and the frequency are not changed significantly in our study. While in LCO, increasing the air speed will increase the vibration amplitude, see *Figure 8* or *Figure 10* for example. But this is cannot sustain indefinitely, at some point the vibrations will no longer be limited and structural failure will occur.

Creating more curvature in the LCO motion is a possibility. Looking at *Figure 6*, we note the decrease in 3B frequency with increased air speed, but still no involvement in the flutter mechanism. Our first attempt to increase power output was to reduce this frequency without significantly changing other properties.
This was achieved by adding discrete masses to the plate, similar to [21]. In our case the masses were added at two chordwise and three spanwise locations. See *Figure 13*. The inward location was chosen to coincide with the nodal line of 2B mode. Masses added there would not influence this natural mode and frequency. The tip of the plate is a more obvious choice as the point of maximum deflection. Adding masses in the middle of the span, points 478, 58, changes the bending modes only. Masses added at the outside points, 74, 53, 2, 42, influence also the torsion modes. Two mass values were used – 5 gr and 10 gr. [1]

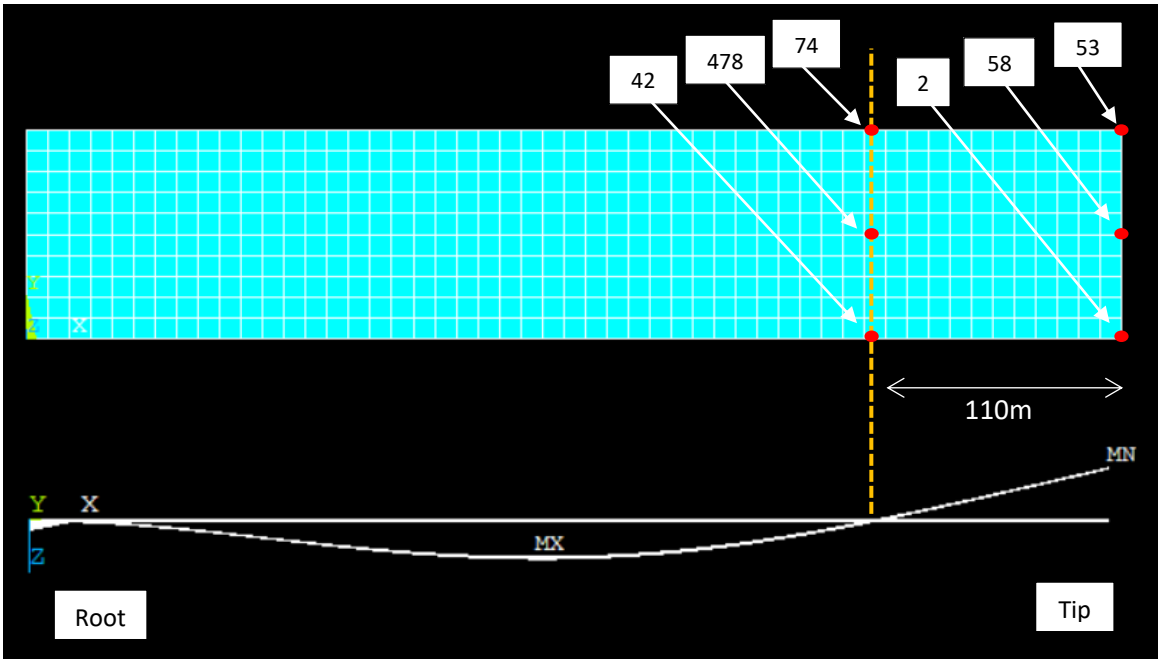

Figure 13: FE Model and Mass Location Points on the Plate

[1] The numbers denoting the spatial locations are chosen to be consistent with the node numbering of the finite element model.

6.1 Verification – Adding Masses to an Empty Plate

To verify the concept, discrete masses were added to the empty plate, at points 74 and 53. See *Figure 14*. The modal analysis results are compared in *Table 2*. ZAERO flutter analysis gives a lower flutter velocity of 10.5 m/sec for 5 gr case and 9.9 m/sec for 10 gr case. See *Figure 15* for a typical vg plot. The dominant flutter mechanism remains 1B and 2B. In addition, a marginally stable behavior can be observed between 20 and 30 m/sec, which involves also the 1T and 3B mode. These results can be potentially beneficial to a more significant piezo elements curvature and thus larger power extraction.

Finally, the calculations were verified with a wind tunnel test. A significant increase in tip accelerations was observed. See *Figure 16* and *Figure 17*. For the 5 gr case, LCO starts at 15.7 m/sec where the tip acceleration increases up to ~300 g. In the 10 gr case, the acceleration goes over 800 g at 15 m/sec, *Figure 17*. In the latter case the vibrations became violent enough to snap off the tip mass. See *Figure 18*.

Note the consistent correlation between the calculated and experimental results. The calculated flutter speed for the empty plate was 14.1 m/sec, *Figure 6*, with experimental value of 18.1 m/sec, *Figure 8*. With the added masses the difference is ~5 m/sec, consistent with analysis results being conservative. As stated before, the difference can be explained by the non-linear nature of the observed oscillations as compared to the linear flutter code which was used for the analysis.
The larger vibration amplitude can potentially increase the power output from the piezo elements, and the reduced LCO air speed can benefit a more practical application of this approach.

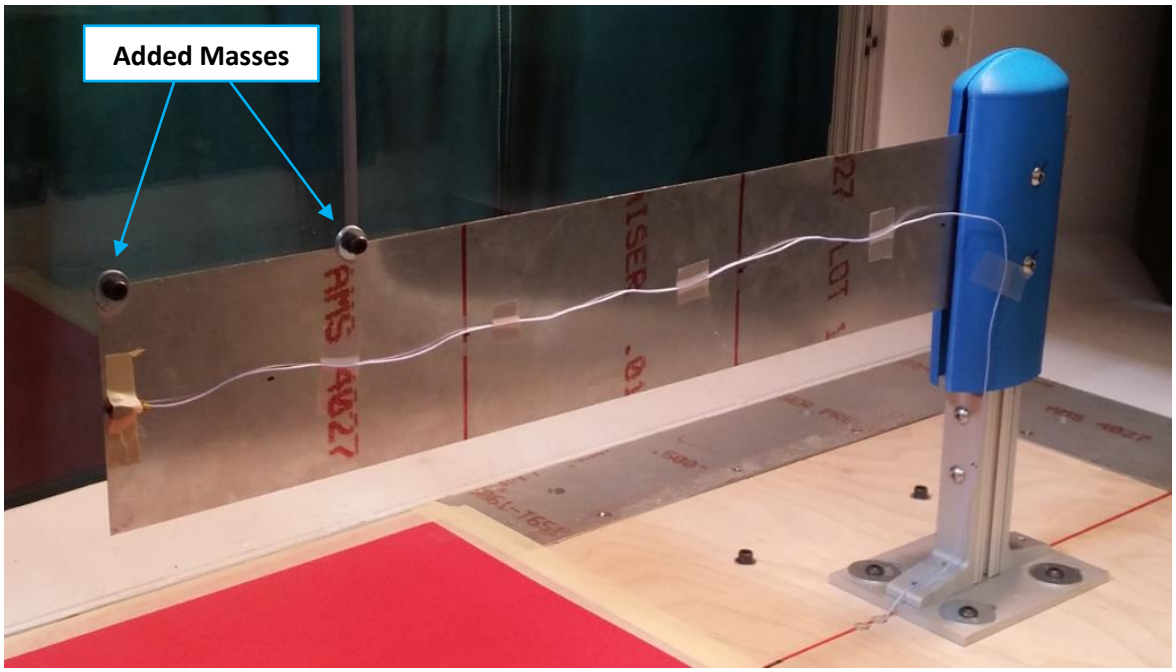

Figure 14: Empty Plate with Added Masses (Shown: 5gr at points 74 and 53)

Table 2: Modal Analysis Results Comparison for an Empty Plate

Mode	Empty Plate		
	f [Hz]		
	Base	5gr at 74, 53	10gr at 74, 53
1B	1.18	0.94	0.8
2B	7.4	6.3	5.8
1T	11.7	9.2	8.5
3B	20.8	17.1	15.25

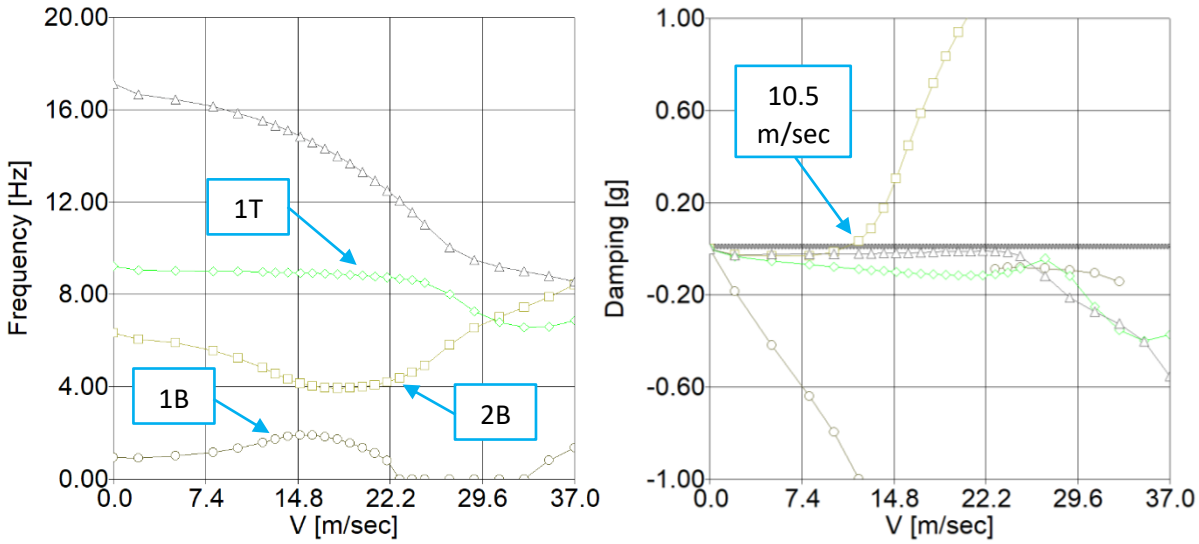

Figure 15: VG Plot for the Empty Plate, 5gr added at points 74 and 53

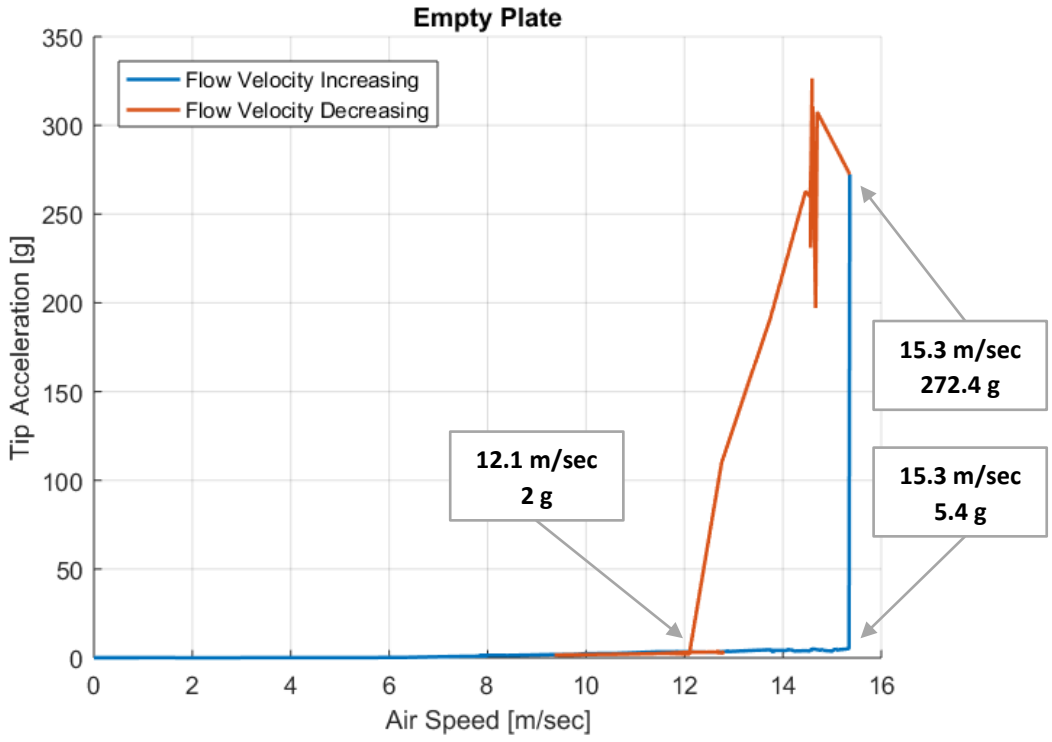

Figure 16: Flutter Test - Empty Plate with 5gr at Points 74, 53

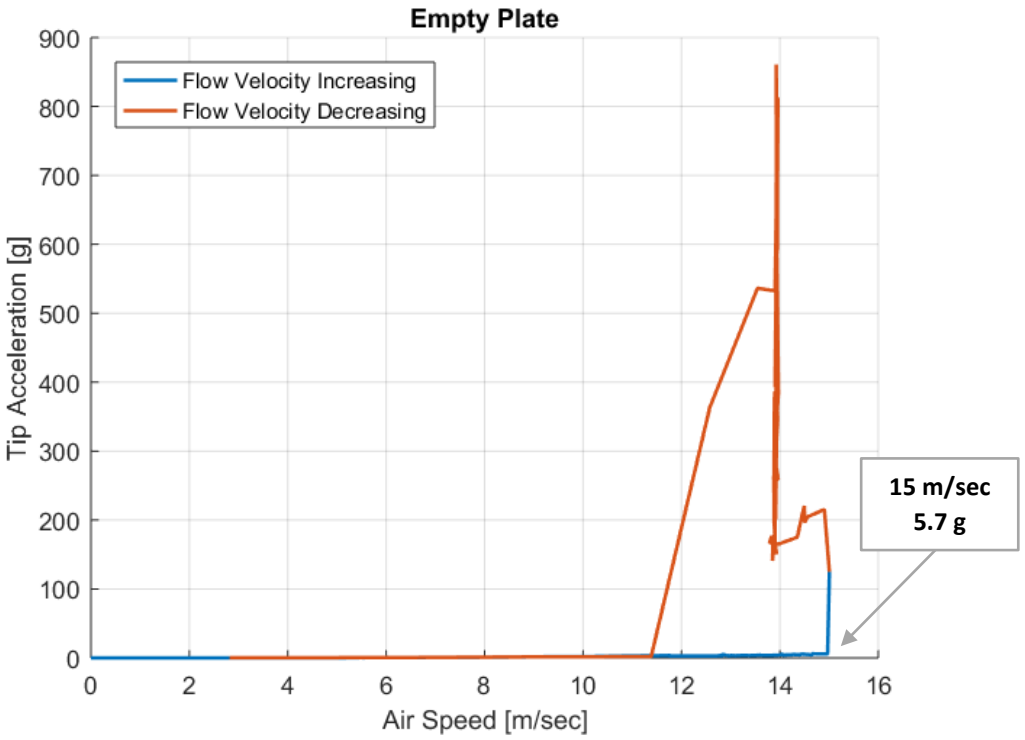

Figure 17: Flutter Test - Empty Plate with 10gr at Points 74, 53

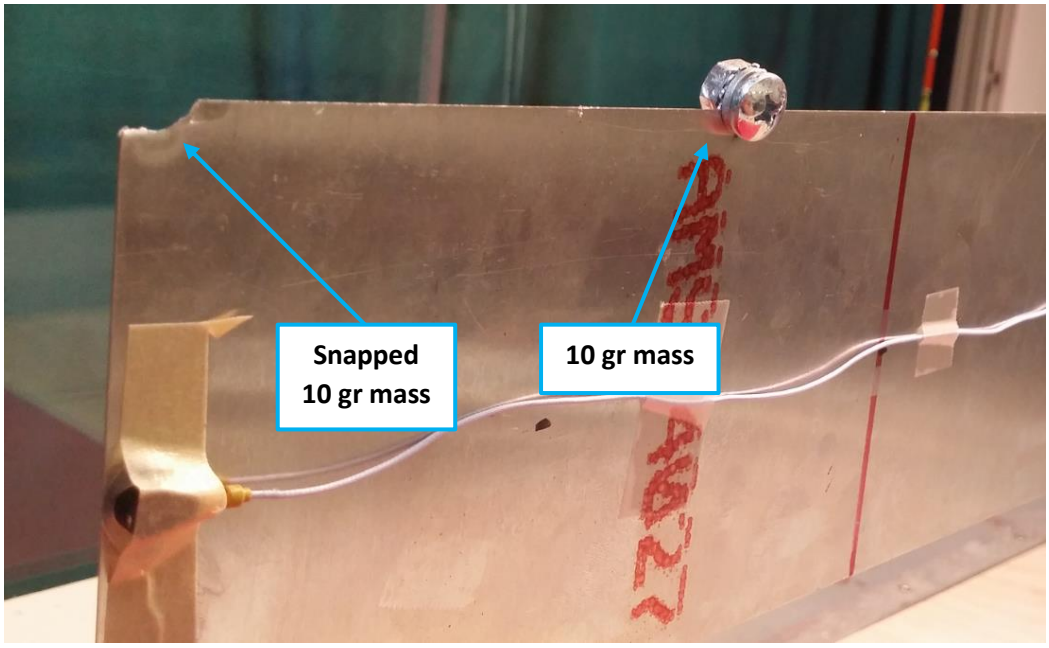

Figure 18: Empty Plate with One Less Mass

6.2 Adding Masses to the Fully Covered Plate

The masses were added to the fully covered plate and the test was repeated. See *Figure 19*. For the 10 gr case, the LCO vibrations engaged at 16.1 m/sec and the flow speed was further increased up to 17.2 m/sec, *Figure 20*, at this point the tip acceleration went over 160g. The maximum power output was 698 μW, *Figure 21*. In the 5gr case, the vibration started at 18.7 m/sec and the speed was increased slightly until 18.9 m/sec, *Figure 22*. The tip acceleration at

maximum speed was 210g. In this case the power output was better – 1104 μW, and the largest so far, *Figure 23*.

Compared to the base line case, we can note several interesting differences. First, the LCO started at lower air speed, which was expected. Potentially the speed can be increased further, and the power output can be compared directly at identical speeds. Due to the concern with the structural integrity of the plate and the test setup, we chose to avoid this.

Second, compared to *Figure 12*, the power output from tip blocks 3, 6 exceeded the output from the root blocks 1, 4. This indicates larger bending curvature involvement at the tip of the plate, compared with the base line case. The output from the root blocks was simultaneously decreased, but overall the power output improved, see *Figure 23*.

Finally, the tip acceleration was lower compared to the empty plate with masses. This can be attributed to significantly larger damping of the fully covered plate. The increased damping can be important in creating a sustainable power generator.

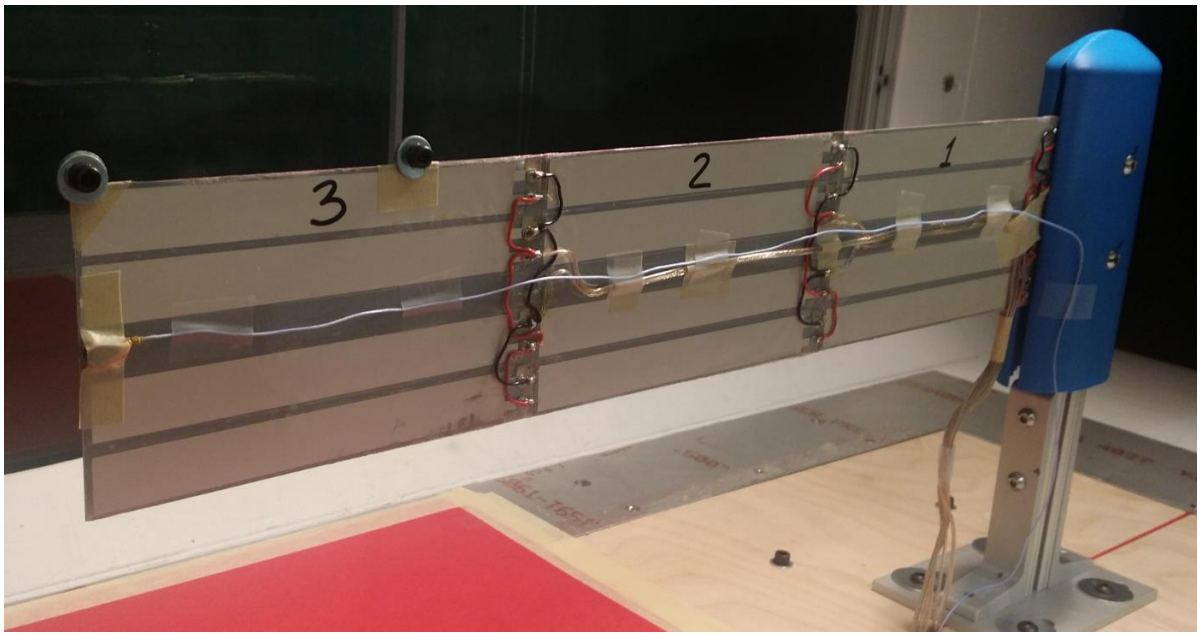

Figure 19: Fully Covered Plate with 5gr Masses at Points 74, 53

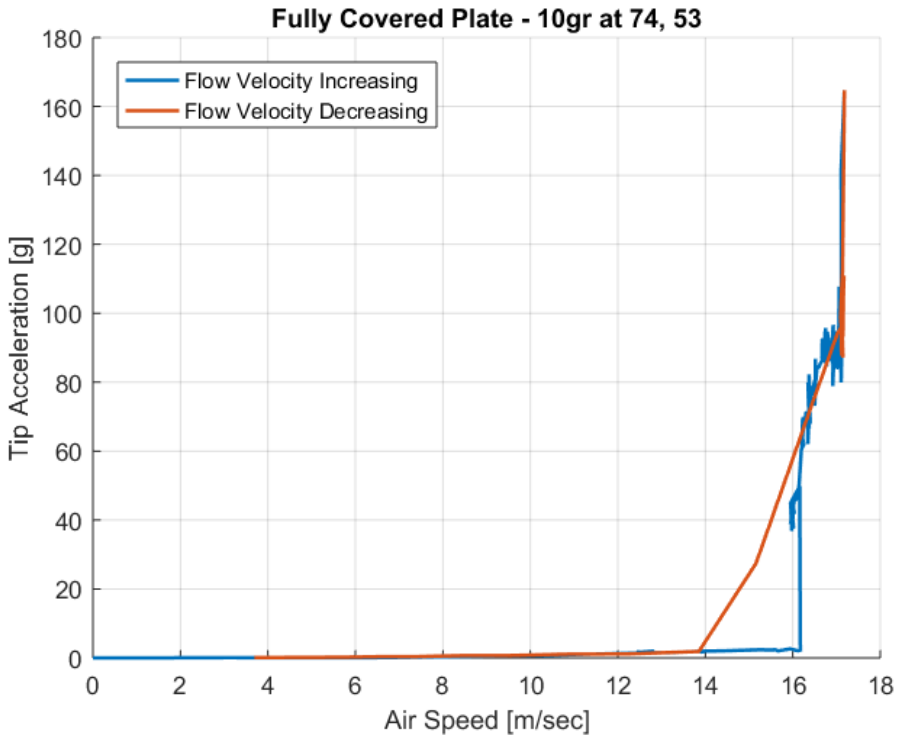

Figure 20: Flutter Test for Fully Covered Plate with 10gr Masses at Points 74, 53

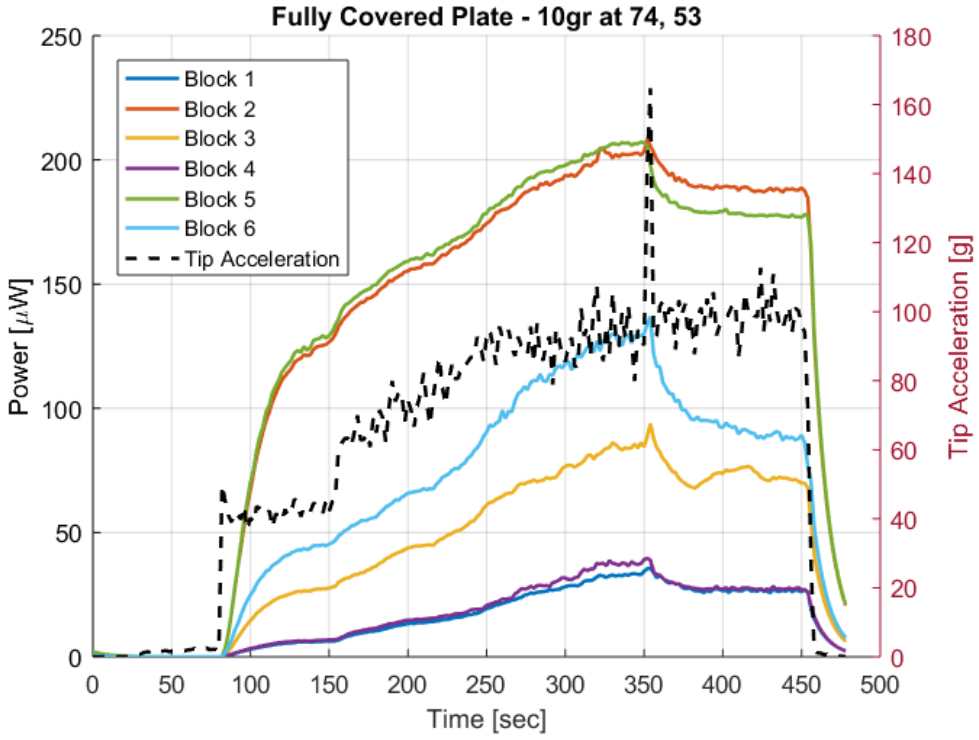

Figure 21: Power Output, Fully Covered Plate with 10gr Masses at Points 74, 53

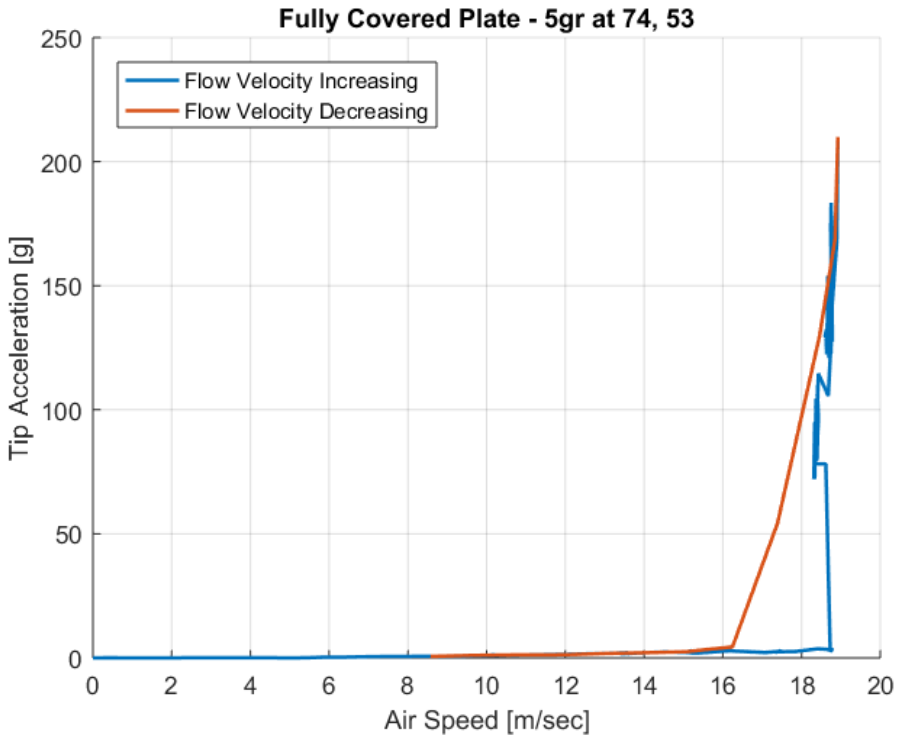

Figure 22: Flutter Test for Fully Covered Plate with 5gr Masses at Points 74, 53

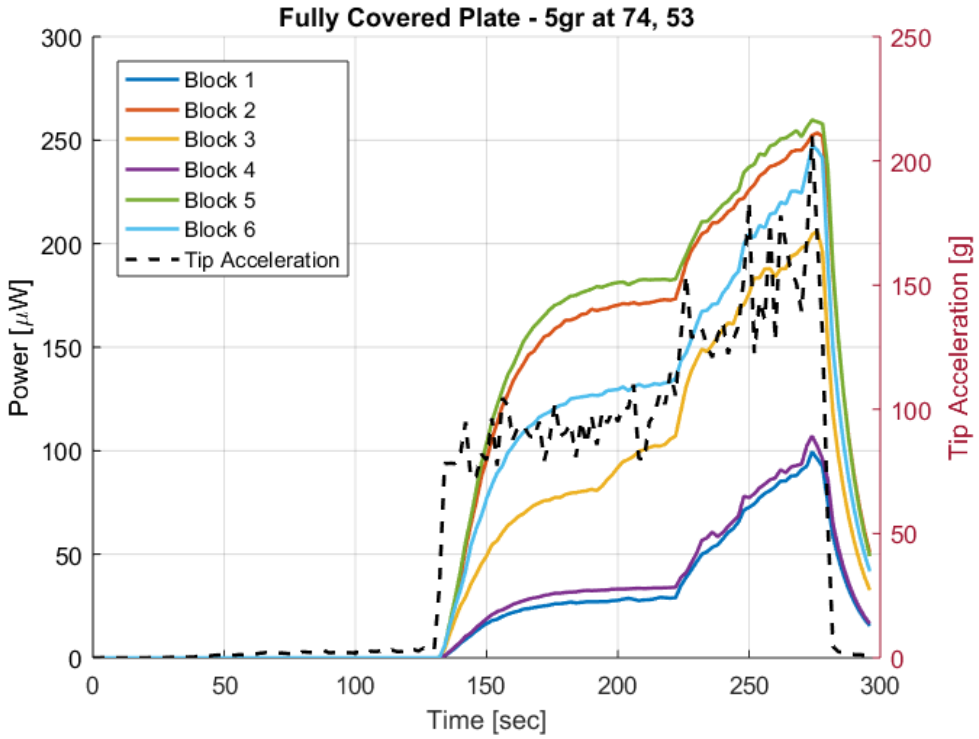

Figure 23: Power Output, Fully Covered Plate with 5gr Masses at Points 74, 53

7 CAN WE DO BETTER? PLACEMENT OF DISCRETE MASSES

In the previous section we discussed a single configuration with added masses which increased the power output compared to that of the plate without added masses. We have demonstrated the potential of this approach. Still it is unclear as to what would be the best location for mass placement. To come closer to the answer, we analyzed and experimented with 14 different cases. See *Table 3* for the summary of these cases, including cases 4 and 5 which were already presented. In this section we will discuss more general trends based on the experiments.

Table 3: Point Masses Configurations

Case #	Added Masses at Points [gr]				
	74	478	53	58	2
Base Line	-	-	-	-	-
1	-	20	-	-	-
2	10	-	-	-	-
3	10	-	-	-	10
4	10	-	10	-	-
5	5	-	5	-	-
6	5	-	10	-	-
7	5	-	-	-	10
8	5	-	15	-	-
9	-	-	-	10	-
10	-	-	10	-	-
11	-	10	-	10	-
12	-	5	-	5	-
13	-	-	-	20	-
14	-	5	-	15	-

For each case, a modal analysis was performed. For several cases, an additional experimental modal analysis was done. See *Table 4*. While the numerical results are for the empty plate with added masses, the test results are for the plate with piezoelectric elements. Note the test frequencies are generally higher than the analytical ones. A flutter/LCO test was also performed for most of the cases. The summary of these test results is presented in *Table 5*. The LCO start air speed is the speed when the acceleration changed suddenly to a higher value and the plate started vibrating visibly. The maximum air speed in test is the highest speed at which we could comfortably accept the level of vibration without endangering the test model. LCO frequency is the dominant frequency of the vibrations.

Table 4: Modal Properties for Various Configurations

Case #	Natural Frequencies [Hz]							
	FE Analysis (Empty)				Experimental (Piezo)			
	1B	2B	1T	3B	1B	2B	1T	3B
Base Line	1.18	7.4	11.7	20.8	1.44	9.95	11.92	22.87
1	0.9	7.4	11.7	18.95	-			
2	1	7.4	8.7	20	-			
3	0.8	5.12	7.96	18.74	-			
4	0.8	5.77	8.5	15.25	-			
5	0.94	6.33	9.23	17.1	-			
6	0.84	5.8	9.11	16.3	-			
7	0.84	5.45	8.51	18.76	-			
8	0.77	5.5	9	15.6	0.91	6.46	10.3	17.94
9	0.88	6.13	11.74	18	-			
10	0.88	5.82	9.9	18.8	1.06	7.2	10.95	20.06
11	0.8	5.96	11.74	16.12	-			
12	0.94	6.47	11.74	17.68	1.11	8.67	11.43	20.46
13	0.74	5.77	11.74	17.47	0.85	7.29	11.4	18.75
14	0.77	5.8	11.74	16.5	-			

An expected outcome from *Table 5* is the lower air speed at which LCO start for all the *modified* cases, compared to the case without an added mass. This extends the practical application of a single aeroelastic system to broader range of air speeds. From the flutter speed at 23.5 m/sec for the base line, we can extend it as low as 15.1 m/sec (case 8 for example). For comparison, below 23.5 m/sec, the base line case experiences no vibrations and therefore no power output.

Table 5: Flutter/LCO Test Results

Case #	LCO Start	Max Air Speed in Test	LCO Frequency	Tip Acceleration		Max Power Output
	[m/sec]		[Hz]	Start	Max	[μW]
Base Line	23.5	23.5	6.4	53.3	77.3	1042
1	-					
2	20.2	21.3	5.6	49	88	724
3	-					
4	16.1	17.2	4.2	82	165	698
5	18.7	18.9	4.8	183	210	1104
6	-					
7	-					
8	15.4	16.8	3.7	61	125	768
9	16.3	17.1	4.7	19	29	793
10	16.8	18.3	4.2	26	76	782
11	16.6	17	4.7	16	22	561
12	18	20.5	5.2	21	43	1001
13	15.1	16.6	4.7	15	22	714
14	15.6	17.4	4.2	16	24	718

In order to further compare between the cases, we introduce "Conversion Coefficient" which normalizes the obtained electric power divided by the invested mechanical energy. This coefficient is dimensionless and is treated as an estimate for power generation efficiency:

$$CC = \frac{P}{\sum(m_{add} \cdot d) \cdot a_{tip} \cdot f_{LCO}} \quad (2)$$

Where: CC – Conversion Coefficient
P – total power generated from piezo elements $[W]$
m_{add} – added mass $[kg]$
d – distance of the added mass from the root* $[m]$
$\sum(m_{add} \cdot d)$ – mass loading of the plate
a_{tip} – tip acceleration $\left[{}^{m}/_{sec^2}\right]$
f_{LCO} – LCO frequency $[Hz]$

*For base line case $m_{add} \cdot d$ is calculated by multiplying the mass of the plate by half chord.

Calculated coefficients for each case are shown in *Figure 24* and *Figure 25*. Separate lines and symbols represent different cases and are plotted against air speed and tip acceleration.

Note the significantly increased efficiency for the center line placed masses, i.e. larger conversion coefficient at lower tip acceleration. Comparing cases 11 and 4, for example (same mass loading), yields ~290% better conversion for case 11, with comparable LCO speed. Adding the masses at the tip adds torsional imbalance to the plate and lowers the torsion mods. While it can result in larger power output, see *Table 5*, it does not support long term sustainability of the structure and the generator. For long term generation we would prefer reduced acceleration and mechanical stresses, and center line placed masses support this.

A direct comparison of the maximum obtained conversion coefficient plotted against mass loading is shown in *Figure 26*, and a better performance is evident for center line placed masses. Larger tip loading results in better performance, however there might be an optimum value with further extension.

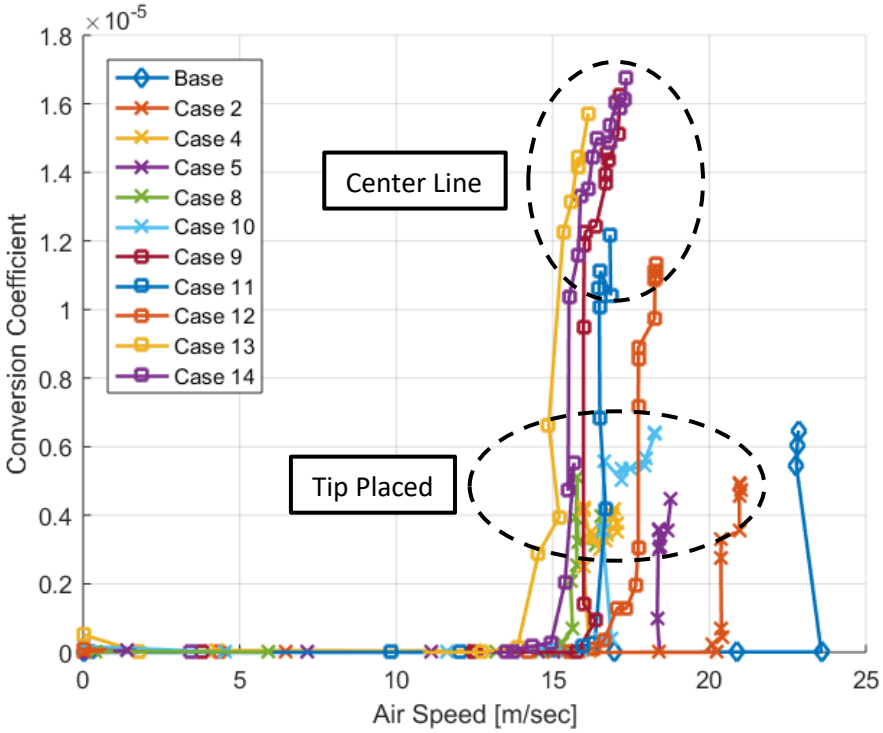

Figure 24: Conversion Coefficient vs. Air Speed

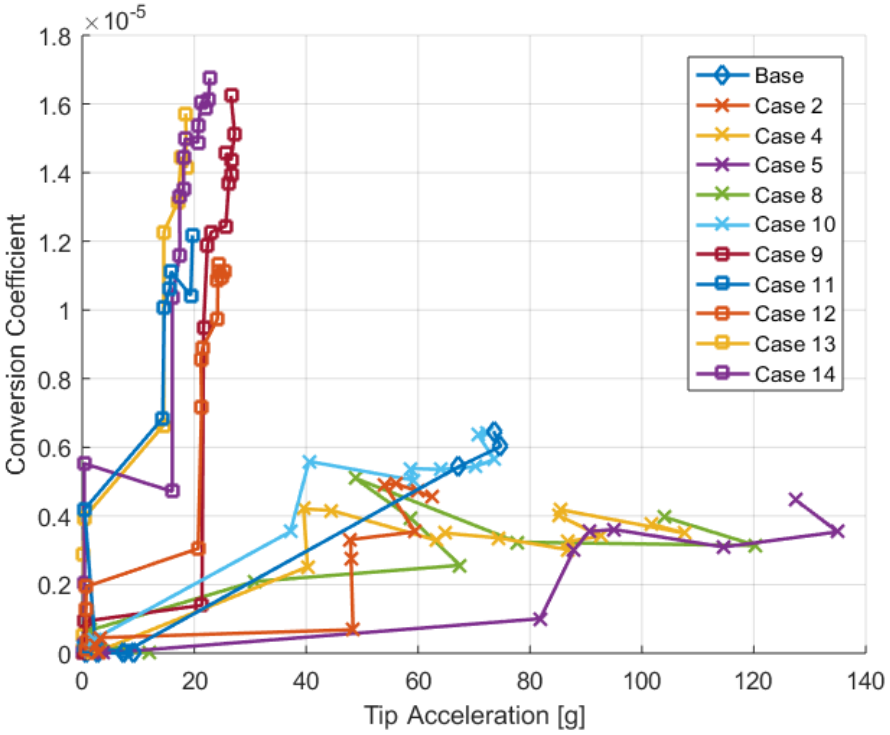

Figure 25: Conversion Coefficient vs. Tip Acceleration

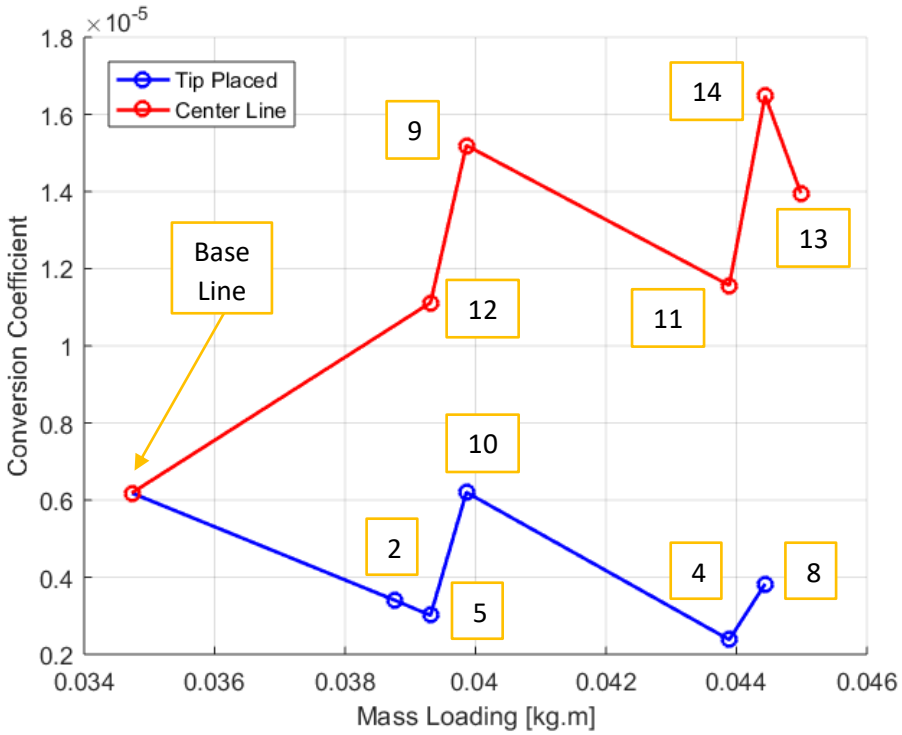

Figure 26: Conversion Coefficient vs. Mass Loading

The test plate had to remain structurally functional throughout the tests. Therefore, the top air speed in the tests was limited. Once we completed the data, the plate served no further purpose. This was an opportunity to check the limits of our setup, i.e. increase the speed until structural failure. This attempt was done with case 12 configuration. The maximum air speed in this test reached 30.7 m/sec with top tip acceleration of 84.1 g. See *Figure 27*. Power output throughout this test is shown in *Figure 28*. The plate did not fail and remained fully functional until the end of the test.

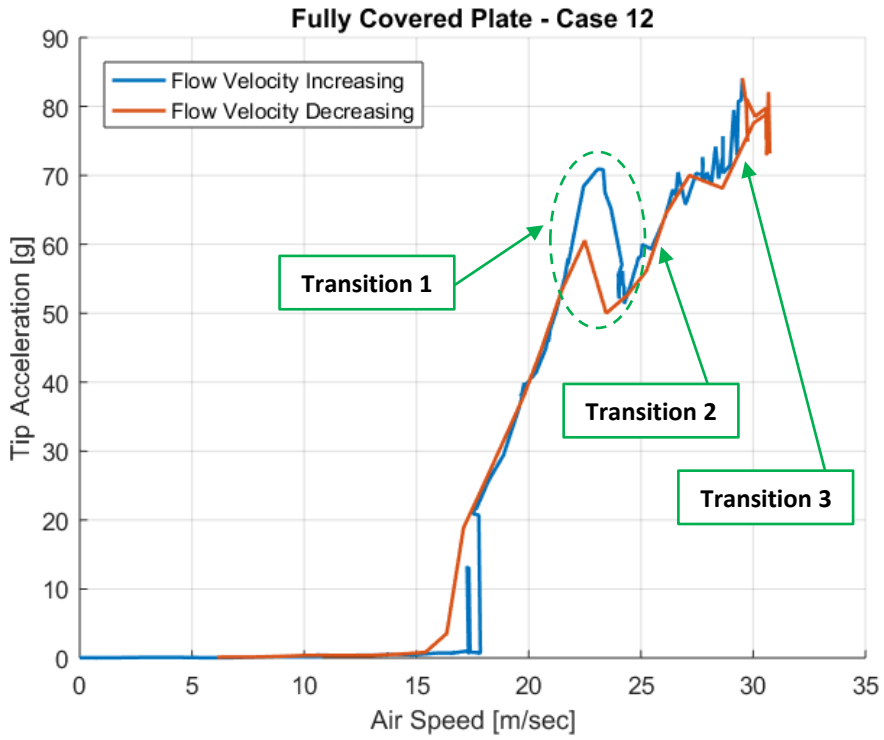

Figure 27: Case 12 - Final Test

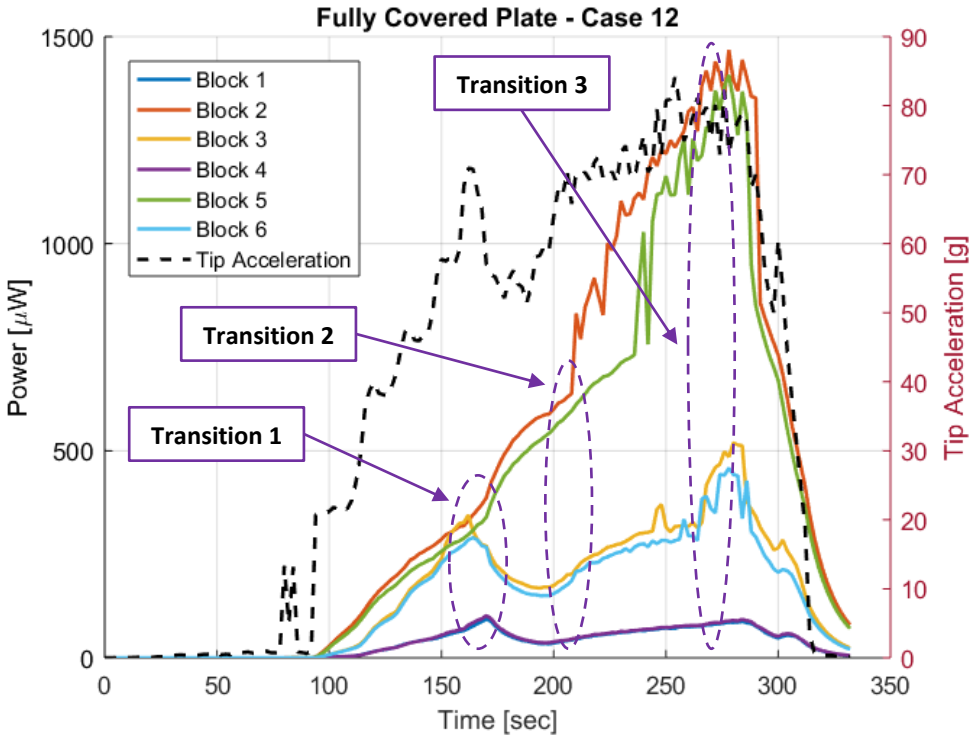

Figure 28: Case 12 - Power Output During Final Test

Note the plunge in acceleration, from 70.8 g to 51.4 g, between 23.3 m/sec and 24.3 m/sec, this transition is repeated while the flow is decreased, with small hysteresis. At 23.3 m/sec the total power output is 1408 μW. Following this point, power output from Blocks 2, 5 is increased, while it is rapidly decreased from the remaining blocks. The next transition occurs at 25.5

m/sec, the power output is increased from all blocks. The final transition occurs at 29.7 m/sec, the power output slopes become higher, and the motion becomes messy. **The total power output at the peak is 3995 µW, all time maximum.** Note the small output from the root blocks during the entire test.

In our tests, the LCO motion consisted mainly of 2nd bending (2B) mode shape, with involvement of the 1st torsional mode (1T). We attributed this to inherent imperfections in the plate, and not perfectly aligned instrumentation and mass placement. This was observed through all the tests.
During the last test however, this behavior changed at ~23.3 m/sec – Transition 1. The vibration shape changed into pure 2B without adverse torsion, and the tip acceleration dropped. This continued through 2nd transition, until ~30 m/sec, when the motion became messy again, without definite mode shape.
FFT analysis of the tip acceleration data confirms our observations. *Figure 29* shows the dominant frequencies immediately after LCO starts. The flutter frequency is 5.2 Hz, which is consistent with past flutter analysis. *Figure 30* and *Figure 31* show the dominant flutter mode, right after the transition into pure 2B. Finally, in *Figure 32* we can see additional frequencies come into play starting at ~30 m/sec.

Despite the transitions in vibrating modes, the plate generated power consistently. The power output increased steadily with the increase in air speed. The plate maintained structural integrity up until 30.7 m/sec, which is **a margin of above 70% over the initial LCO speed of 18 m/sec**. This can be attributed to the high non-linearity of the motion and the large damping of the fully covered plate.

Figure 33 shows the calculated Conversion Coefficient for the final test. Compared to the initial Case 12 test, the air speed was increased faster, without fully charging the capacitors at LCO start speed. At larger air speeds the transitions and slope changes follow the trends in *Figure 28*, although these changes are not fully understood.

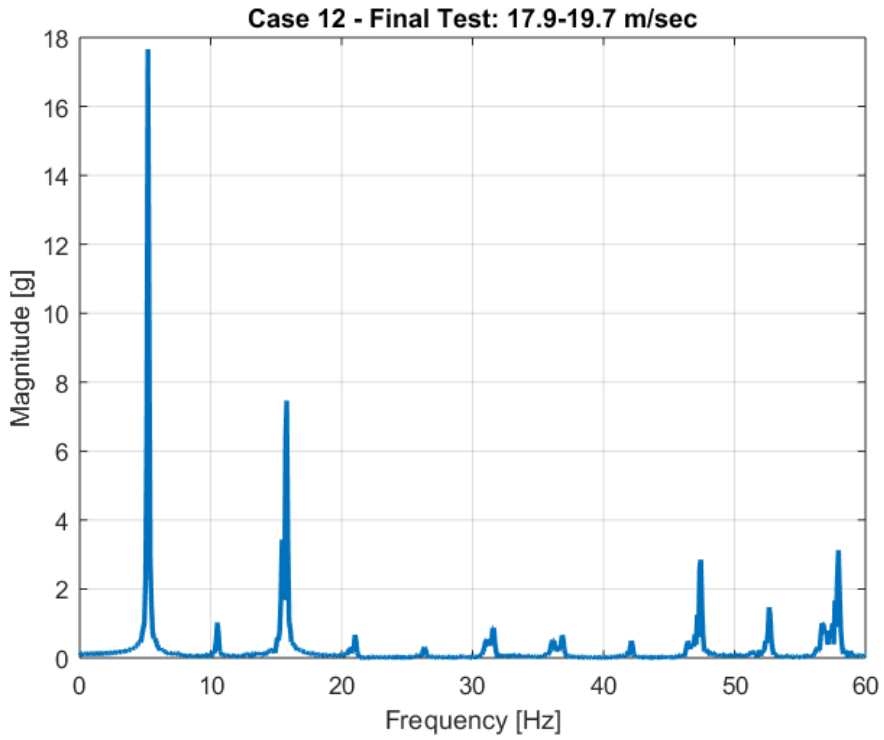

Figure 29: Case 12, Final Test - LCO Start

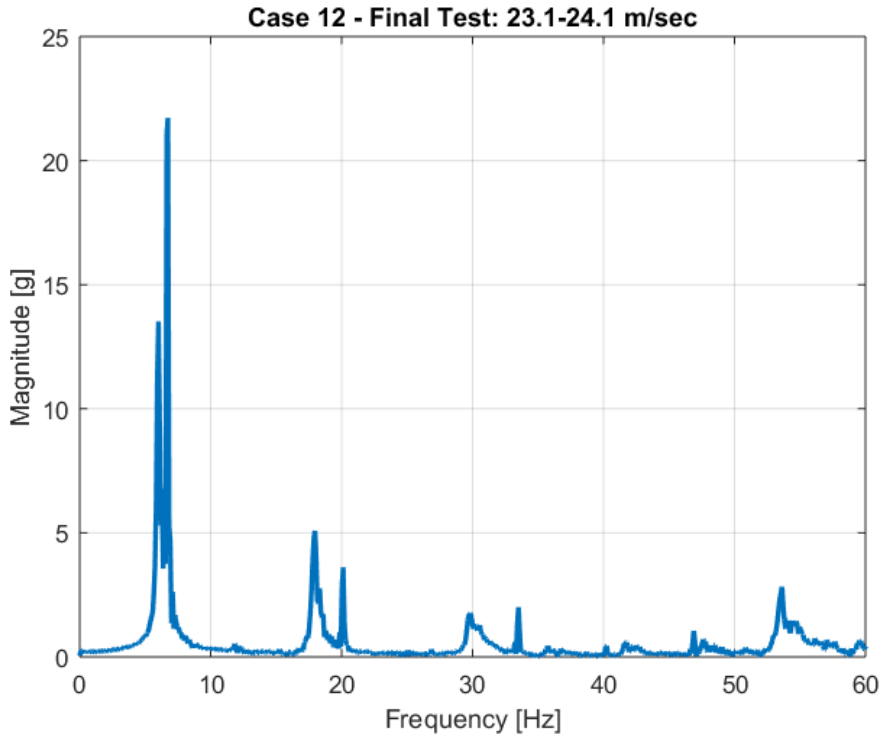

Figure 30: Case 12, Final Test - Before Transition 1

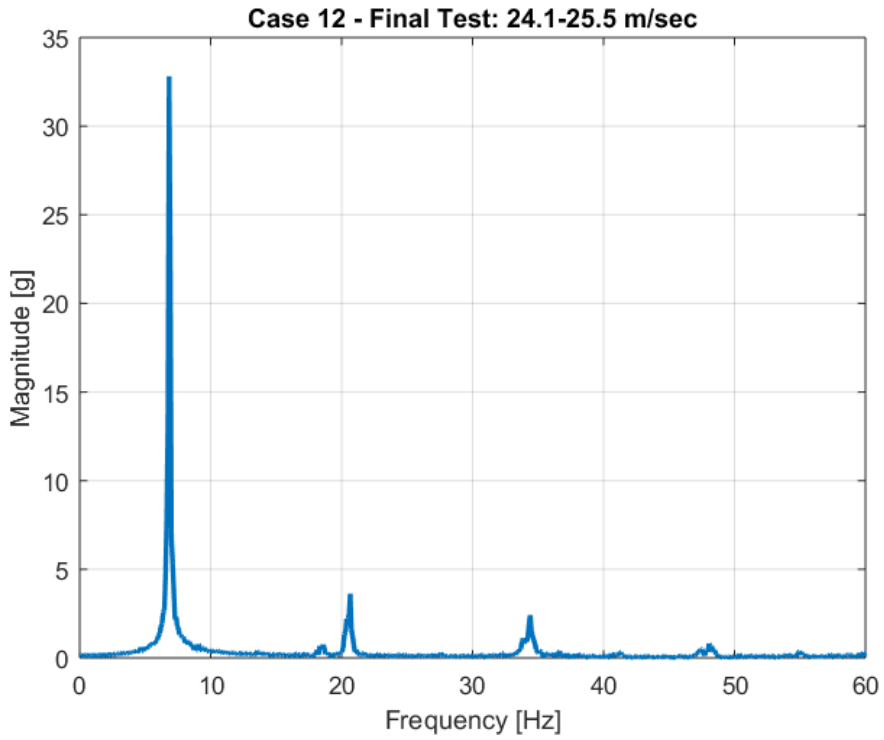

Figure 31: Case 12, Final Test - Transition 1

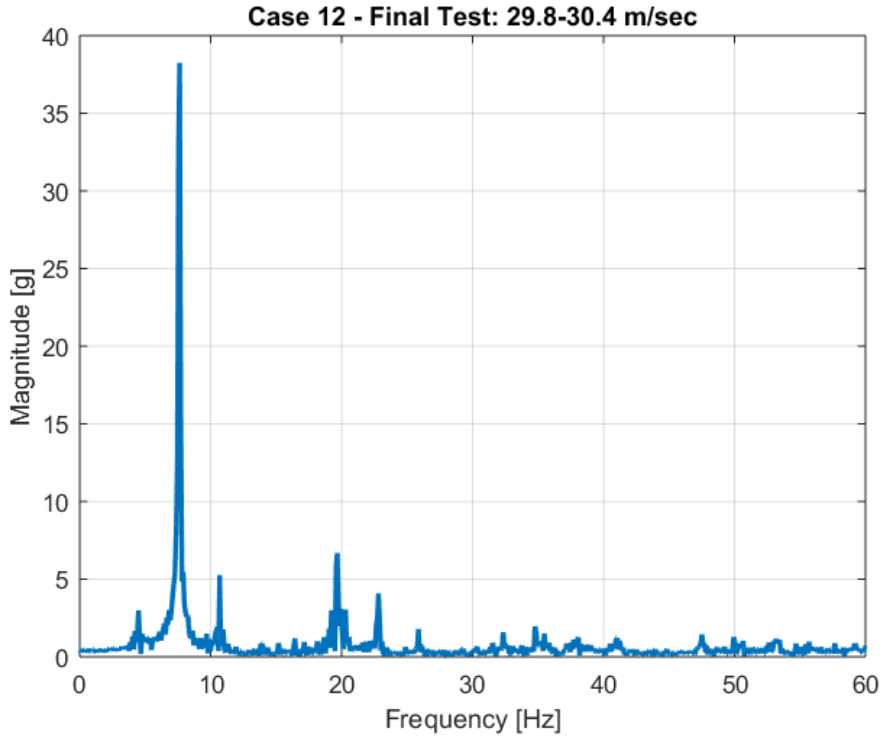

Figure 32: Case 12, Final Test - Transition 3

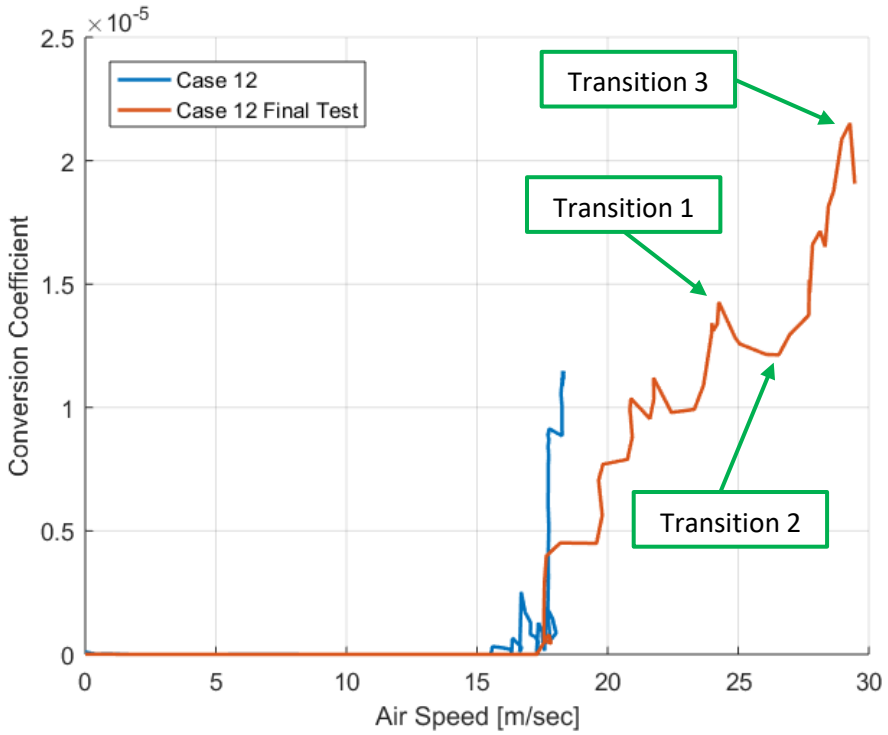

Figure 33: Conversion Coefficient for Case 12, Final Test

8 CAN WE DO EVEN BETTER? MORE EFFICIENT PIEZOELECTRIC ELEMENTS

In previous sections we increased the efficiency of piezo-aeroelastic power generator by changing the dynamics of the basic structure and improving the aeroelastic behavior. In this section we will explore the benefits of using more efficient piezoelectric elements.

An additional plate was assembled. The plate is geometrically identical and is made from the same aluminum strip as the original one. The plate was instrumented with the same piezoelectric elements at the root and the tip, i.e. blocks: 1, 3, 4, 6. The area of block 2, the maximum power output, was covered with different piezo elements – DuraAct P-876.A11, manufactured by PI (www.piceramic.com). See comparison in *Table 6*.

PI elements have higher piezoelectric strain constant (d_{31}), piezoelectric voltage constant (g_{31}) and electromechanical coupling factors (k_{31}, k_t). These are the influencing factors for energy harvesting applications [3]. On the other hand, these elements are much stiffer and heavier, and might limit the vibrations. Due to the added stiffness, see *Figure 34*, we chose to leave the block 5 area uncovered. In addition, the two types of elements have different form factor, see *Table 6*, therefore an area which was previously covered by 4 TE elements, is now covered by 9 PI elements, *Figure 35*.

After mounting the plate in the tunnel, a basic modal test was performed, the results are presented in *Table 7*. The plate is stiffer and more damped compared to the original plates, see *Table 1*.

Table 6: Piezoelectric Elements Comparison

	TE	PI
Model	DT4-028K/L	P-876.A11
Type	PVDF	Ceramic
Dimensions [mm]	171x22	61x35
Dimensions (Active) [mm]	156x19	50x30
Thickness [mm]	0.157	0.4
Elastic Modulus [GPa]	3	16.4
Density [kg/m^3]	1780	7800
d_{31} [m/V]	$23 \cdot 10^{-12}$	$1.867 \cdot 10^{-10}$
g_{31} [Vm/N]	$216 \cdot 10^{-3}$	$1.205 \cdot 10^{-2}$
k_{31} [%]	12	37
k_t [%]	14	49

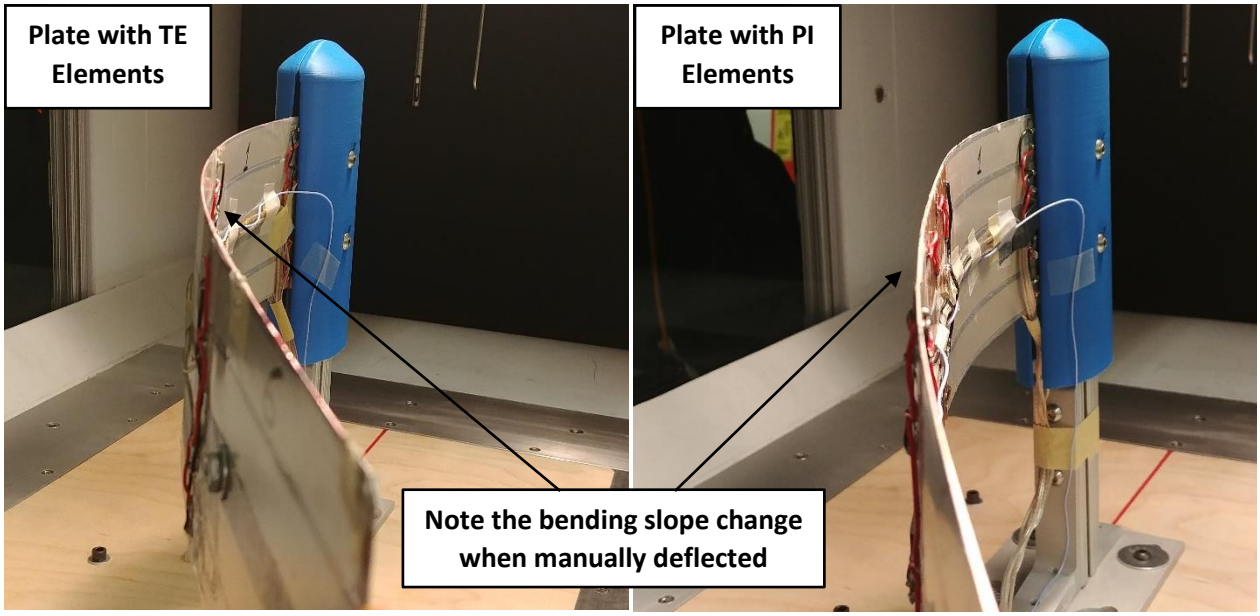

Figure 34: Visual Stiffness Comparison, TE vs. PI

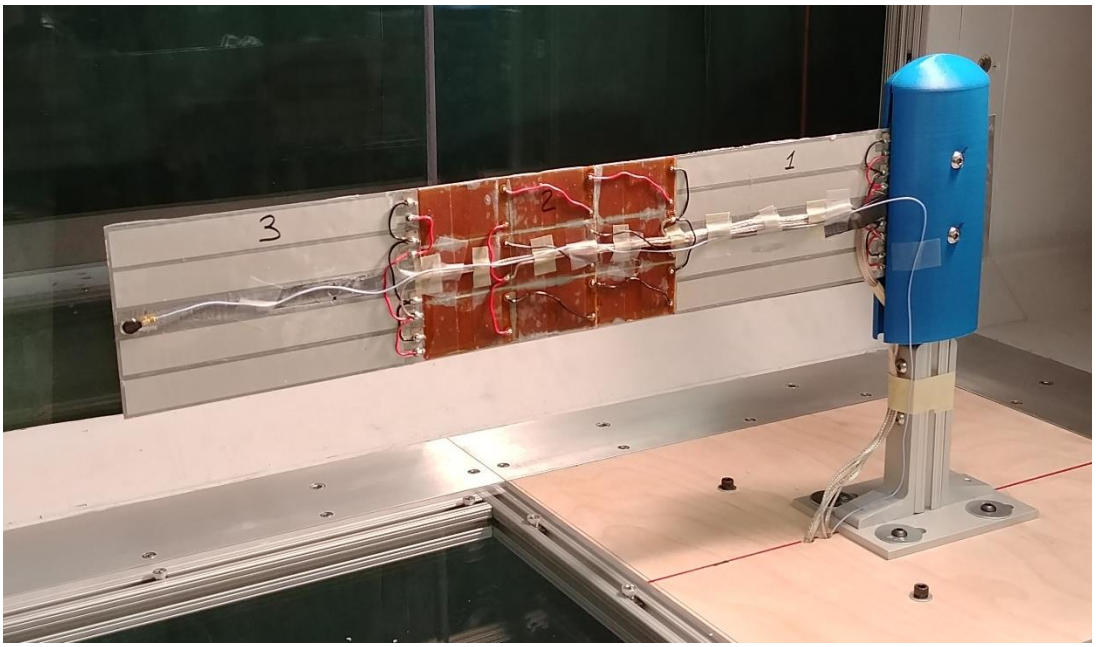

Figure 35: New Plate with PI Elements

Table 7: Modal Test Results for PI Plate

Mode	f [Hz]	Damp [%]
1B	1.41	3.49
2B	10.97	3.15
1T	13.78	1.4
3B	25.75	3.86

For direct comparison, we used case 12 and case 14 mass configuration. Case 12 was chosen due to the extensive testing of the original plate, and case 14 is the most power efficient.

In Case 12, the LCO started at 32.6 m/sec with deliberate deflection. See *Figure 36*. LCO did not start at lower speeds despite the repeated deflection attempts. This can be due to the increased stiffness and damping of this setup. Note the large hysteresis when decreasing flow velocity, the vibrations stopped completely at 18.4 m/sec, resembling the behavior in initial tests, *Figure 9*. The power output from this case is shown in *Figure 37*. Note the significant increase in power output from PI elements at the mid location, **the peak output is 4060 µW** (for PI elements only). The maximum power output in this case is **5262 µW**. The addition of 1202 µW from the remaining TE elements is comparable to our previous experience with case 12, see *Table 5* and *Figure 28*.

In case 14 configuration, the power was generated in two instances, see *Figure 38*. The LCO started at 22.6 m/sec, then the air speed was reduced until vibrations stopped. Next LCO vibrations started at 17.4 m/sec with deliberate initiation. The maximum tip acceleration during this test remained under 40 g, which resembles the values observed with the original plate, see *Table 5*. In the end of this test the PI elements were separated from the plate. See *Figure 39*. No structural failure occurred, and the test ended safely. The initial separation of the elements occurred ~180 sec into the test, see *Figure 40*, when a plunge in power output was recorded. At ~195 sec the tip acceleration and power output both increased. The plate began vibrating with increased amplitude - 33.6 g (21 g before) and the power output increased again. During these

transitions the air speed did not change and remained ~18 m/sec. Before the separation, power output from PI elements was 2875 µW, and the total output resulted in 3681 µW.

The increased amplitude was due to the loss of plate stiffness after elements separation. We believe that the epoxy layer, which bonded the elements to the plate, started failing during case 12 test, and finished during case 14. Interestingly, the power output for PI elements after the separation returned to its levels before the separation. This time however, the power generation was due to elements flapping in the air and not oscillating with the plate.

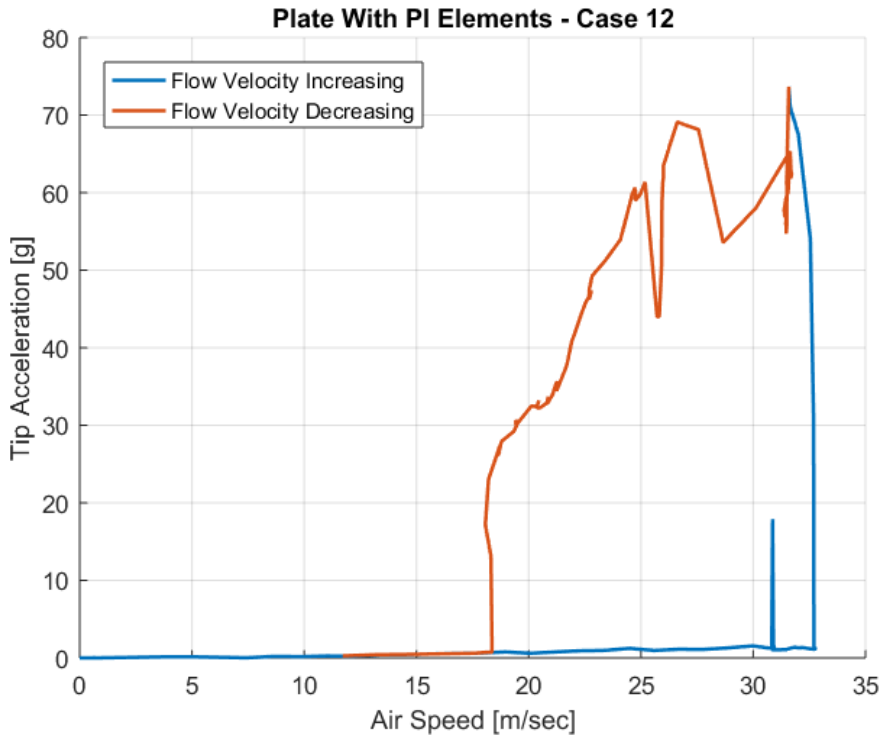

Figure 36: Flutter Test with PI Elements - Case 12

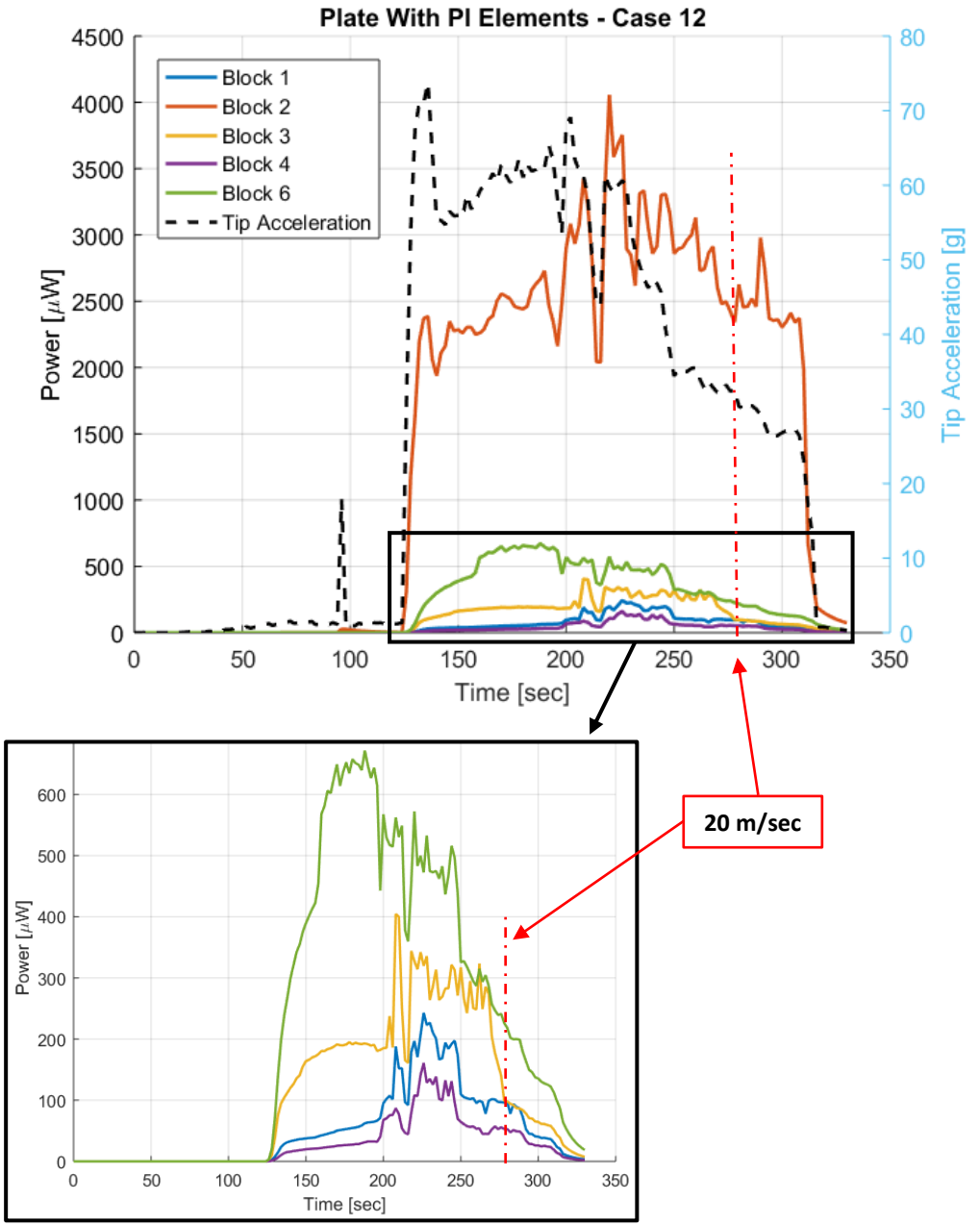

Figure 37: Power Output, Case 12 with PI Elements

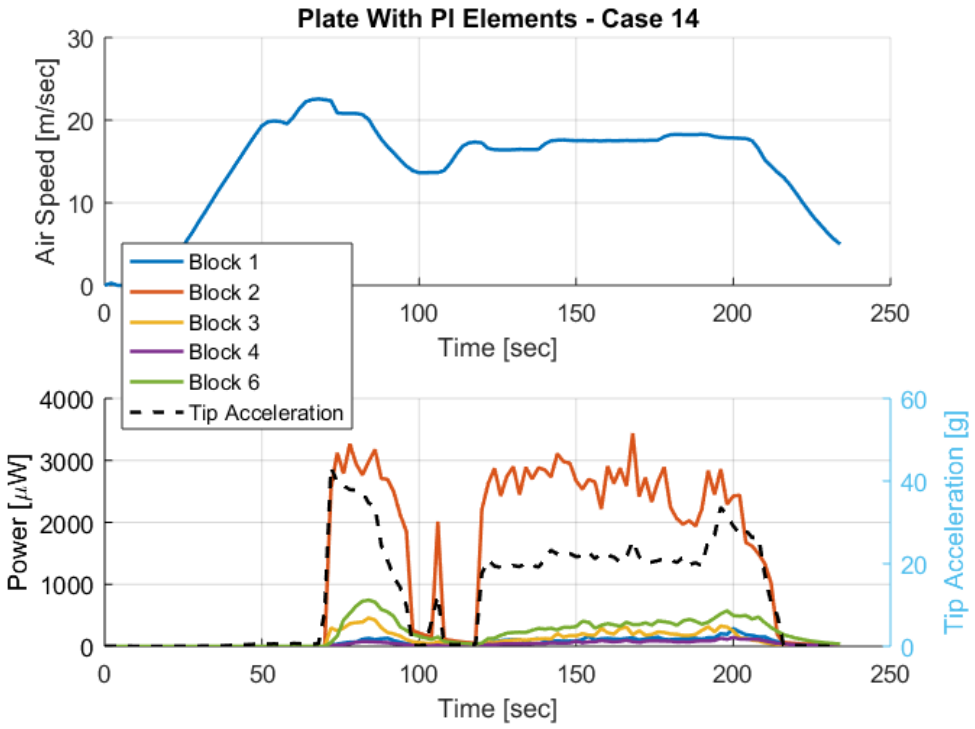

Figure 38: Power Output, Case 14 with PI Elements

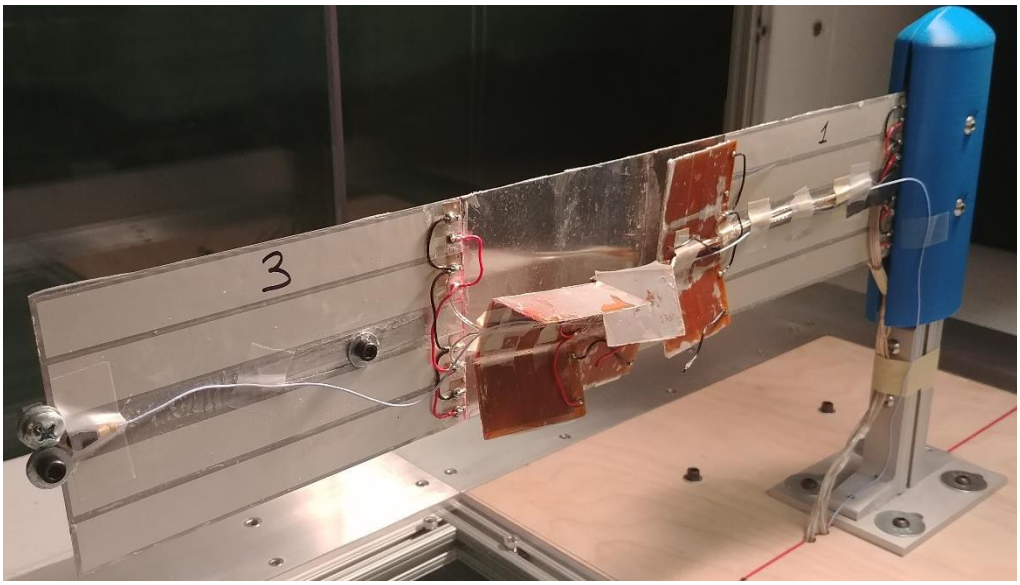

Figure 39: PI Plate, End of Case 14 Test

Figure 40: PI Plate, Case 14, Final Test

9 SUMMARY

In this work we explored the possibilities of improving the conversion efficiency of an aeroelastic power generator. By placing small discrete masses on the plate, we were able to increase the efficiency by ~260%, while simultaneously reducing the required air speed from 23.5 m/sec to 15.6 m/sec (Case 14 vs. Base Line for example).

The non-linear nature of LCO allows us to expand the useful range of air speeds from a single onset to a wider range, i.e. 23.5 m/sec in the base line case to 18 m/sec – 30.7 m/sec for Case 12. The plate survived these tests without structural failure, and this opens possibilities for practical energy harvesters based on non-linear aeroelastic effects and piezo-elements.

Center line placed masses are preferred for sustainable power generation. Reduced frequency torsional modes will subject the structure to higher loads without contributing to a better conversion.

While in LCO, the plate experiences variations in deflection shapes (see Case 12 final test) and, as a result, variations in power generation. Future work might include an effort to understand these trends.

Several additional observations we made during the tests are highlighted here:

- The tip area is usually not exploited in vibrational energy harvesting tests. By adding small masses towards the tip of the plate, this area can be more significant than the root.
- For sustainable power generators, a damped structure is preferred.
- For highly flexible structures, like the plate in our case, low-stiffness PVDF piezo-elements are the preferred choice. Despite their lower efficiency, these elements will not limit the full potential of power generation. PVDF elements are also cost efficient.

Future adaptation of this work might include a feedback mechanism which will control the spanwise mass location at several chord locations. This allows one to match the dynamics of the plate to the ambient wind speeds for favorable power generation.

COPYRIGHT STATEMENT

10 REFERENCES

[1] S. R. Anton and H. A. Sodano, "A review of power harvesting using piezoelectric materials (2003-2006)," *Smart Materials and Structures,* vol. 16, no. R1-R21, 2007.

[2] D. Li, Y. Wu, A. Da Ronch and J. Xiang, "Energy Harvesting by Means of Flow-Induced Vibrations on Aerospace Vehicles," *Progress in Aerospace Sciences,* vol. 86, pp. 28-62. http://dx.doi.org/10.1016/j.paerosci.2016.08.001, 2016.

[3] H. Li, C. Tian and D. Z. Deng, "Energy harvesting from low frequency applications using piezoelectric materials," *Applied Physics Reviews,* vol. 1, no. 041301 doi: 10.1063/1.4900845, 2014.

[4] Z. Guangyi, G. Shiqiao and L. Haipeng, "A utility piezoelectric energy harvester with low frequency and high-output voltage: Theoretical model, experimental verification and energy storage," in *AIP Advances 6, 095208: doi; 10.1063/1.4962979,* Beijing, 2016.

[5] J. W. Cryns, B. K. Hatchell, E. Santiago-Rojas and K. L. Silvers, "Experimental Analysis of a Piezoelectric Energy Harvesting System for HArmonic, Random, and Sine on Random Vibration," *Advances in Acoustics and Vibration,* vol. 2013, no. Article ID 241025 http://dx.doi.org/10.1155/2013/241025, 2013.

[6] D. Motter, J. V. Lavarda, F. A. Dias and S. da Silva, "Vibration Energy Harvesting Using Piezoelectric Transducer and Non-Controlled Rectifiers Circuits," *ABCM,* vol. XXXIV, no. Special Issue 2012, 2012.

[7] J. M. McCarthy, S. Watkins, A. Deivasigamani and S. J. John, "Fluttering Energy Harvestersin the Wind: A review," *Journal of Sound and Vibration,* vol. 361, pp. 355-377. http://dx.doi.org/10.1016/j.jsv.2015.09.043, 2016.

[8] A. Abdelkefi, "Aeroelastic Energy Harvesting: A Review," *International Journal of Engineering Science* , vol. 100, pp. 112-135. http://dx.doi.org/10.1016/j.ijengsci.2015.10.006, 2016.

[9] J. A. Dunnmon, S. C. Stanton, B. P. Mann and E. H. Dowell, "Power extraction from aeroelastic limit cycle oscillations," *Journal of Fluids and Structures,* p. doi:10.1016/j.jfluidstructs.2011.02.003, 2011.

[10] A. Abdelkefi, A. H. Nayfeh and M. R. Hajj, "Design of piezoaeroelastic energy harvesters," *Nonlinear Dynamics,* vol. 68, no. DOI 10.1007/s11071-011-0233-x, pp. 519-530, 2012.

[11] A. Abdelkefi, A. H. Nayfeh and M. R. Hajj, "Enhancement of power harvesting from piezoaeroelastic systems," *Nonlinear Dynamics,* vol. 68, no. DOI 10.1007/s11071-011-0234-9, pp. 531-541, 2012.

[12] M. Bryant and E. Garcia, "Modeling and Testing of a Novel Aeroelastic Flutter Energy Harvester," *Journal of Vibration and Acoustics,* vol. 133, no. 011010-1 DOI: 10.1115/1.4002788, 2011.

[13] V. C. Sousa, M. d. M. Anicezio, C. D. Marqui Jr and A. Erturk, "Enhanced aeroelastic energy harvesting by exploiting combined nonlinearities: theory and experiment," *Smart Materials and Structures,* vol. 20, no. 094007 doi:10.1088/0964-1726/20/9/094007, 2011.

[14] D. M. Tang and E. H. Dowell, "Aeroelastic response and energy harvesting from a cantilevered piezoelectric laminated plate," *Journal of Fluids and Structures,* vol. 76, no. https://doi.org/10.1016/j.jfluidstructs.2017.09.007, pp. 14-36, 2018.

[15] M. Pineirula, O. Doare and S. Michelin, "Influence and optimization of the electrodes position in a piezoelectric energy harvesting flag," *Journal of Sound and Vibration,* vol. 346, no. http://dx.doi.org/10.1016/j.jsv.2015.01.010, pp. 200-215, 2015.

[16] C. De Marqui Jr., D. Tan and A. Erturk, "On the electrode segmentation for piezoelectric energy harvesting from nonlinear limit cycle oscillations in axial flow," *Journal of Fluids and Structures,* vol. 82, no. https://doi.org/10.1016/j.jfluidstructs.2018.07.020, pp. 492-504, 2018.

[17] H. C. Lin, P. H. Wu, I. C. Lien and Y. C. Shu, "Analysis of an array of piezoelectric energy harvesters connected in series," *Smart Materials and Structures,* vol. 22, no. doi:10.1088/0964-1726/22/9/094026, 2013.

[18] J. W. Moon, H. J. Jung, K. H. Baek, D. Song, S. B. Kim, J. H. Kim and T. H. Sung, "Optimal design and application of a piezoelectric energy harvesting system using multiple piezoelectric modules," *Journal of Electroceramics,* vol. 32, no. DOI 10.1007/s10832-014-9934-0, pp. 396-403, 2014.

[19] A. M. Ain, L. KokSwee and M. A. Noraini, "PIEZOELECTRIC ENERGY HARVESTING RECTIFYING CIRCUITS COMPARISON," *ARPN Journal of Engineering and Applied Sciences,* vol. 11, no. 10, 2016.

[20] J. Dicken, P. D. Mitcheson, I. Stoianov and E. M. Yeatman, "Power-Extraction Circuits for Piezoelectric Energy Harvesters in Miniature and Low-Power Applications," *IEEE Transactions on Power Electronics,* vol. 27, no. 11, pp. 4514-4529, 2012.

[21] R. M. Howell, A. D. Lucey and M. W. Pitman, "The effect of inertial inhomogeneity on the flutter of a cantilevered flexible plate," *Journal of Fluids and Structures,* vol. 27, no. doi:10.1016/j.jfluidstructs.2010.11.014, pp. 383-393, 2011.

[22] D. M. Tang, D. Levin and E. H. Dowell, "Experimental and Theoretical Correlations for Energy Harvesting from a Large Flapping Flag Response," *Journal of Fluids and structures,* vol. 86, pp. 290-315. https://doi.org/10.1016/j.jfluidstructs.2019.02.018, 2019.